Workability, strength and shrinkage of ultra-high-performance seawater, sea sand concrete with different OPC replacement ratios

Shameer Saleh[a], Ying-Lei Li[a], Ehab Hamed[a], Aziz Hasan Mahmood[a] and Xiao-Ling Zhao[a,b]*

[a]School of Civil and Environmental Engineering, UNSW Sydney, Kensington, NSW 2052, Australia

[b]Department of Civil and Environmental Engineering, The Hong Kong Polytechnic University, Hong Kong, China

(*Corresponding Author. Email: xiaolin.zhao@unsw.edu.au)

Abstract

An experimental investigation on the chemical, physical, mechanical, and shrinkage of seawater and sea sand-based ultra-high-performance concrete (UHP-SWSSC) with supplementary cementitious materials (SCM) (i.e., slag and silica fume) is reported. Several mixes were designed with varying proportions of SCMs (25%, 37.5%, 50%, and 62.5% of binder), aggregate source, and water-to-binder ratio. Heat evolution, density, workability, compressive strength development, and long-term autogenous and drying shrinkage of UHP-SWSSC were monitored. Seawater accelerates cement hydration as reflected in the heat evolution, and consequently, dictates the early-age strength, and autogenous shrinkage. SCM addition although limits the early-age strength development offers a comparable 90 days strength. The chloride content increases from marine resources and may limit the application to non-structural components. Nonetheless, a UHP-SWSSC mix with 50% OPC replaced by 37.5% slag and 12.5% silica fume is recommended in this study, which can achieve satisfactory workability, long-term strength, and shrinkage properties.

Keywords: Ultra-high-performance seawater sea sand concrete, OPC replacement ratio, water-to-binder ratio, strength, workability, shrinkage.

1. Introduction

Being the most widely utilized construction material, the demand for ordinary Portland cement (OPC) concrete in infrastructure industries has significantly increased over the past few decades. The total amount of cement produced worldwide in the year 2020 was 4.1 billion tons, which is almost three-fold compared to the cement production in 1995 [1]. This huge demand and consequently, the production, has not only exacerbated the scarcity of natural resources (i.e., fresh water and river sand) by overexploiting them as raw materials but also worsened the ecological balance through substantial CO_2 emission in the manufacturing of OPC [2]. An alternative to the consumption of limited natural resources is to utilize seawater and sea-sand concrete (SWSSC) which can be a sustainable substitute to depleting fresh water and river sand. In addition, proper management of hazardous industrial by-products, including ground granulated blast furnace slag, silica fume, fly ash, etc. is a potential challenge [3] with a noteworthy possibility of being reused and recycled as supplementary cementitious materials (SCMs) in concrete manufacture. Blast furnace slag and silica fume are by-products of steel and ferrosilicon manufacturing industries, respectively [4], which possess pozzolanic reactivity and thus, may be used as SCMs by replacing OPC in SWSSC. However, concerns remain with the use of chloride enriched marine resources in concrete as this can potentially stimulate corrosion in the embedded reinforcing steel. Alternative hybrid construction approaches utilizing seawater and sea-sand concrete and corrosion resistant materials such as fiber reinforced polymers (FRP) and stainless steel, nonetheless, possess an enormous potential in future sustainable construction practice e.g., [5-9], particularly in the coastal regions.

Relevant studies have demonstrated that the utilization of sea-sand [2, 10] and seawater [11-13] in concrete increases early-age compressive strength, lowers long-term compressive strength [14,

15], makes the concrete less workable [16], and increases drying shrinkage [17, 18] compared to fresh water and river sand counterparts due to the salt and sea-shell contents present in them. Application of seawater to cure SWSSC reduces the compressive strength and modulus of elasticity as opposed to conventional freshwater curing [15]. The expansion of SWSSC because of alkali-silica reaction (ASR) which ultimately induces cracking in concrete can be substantially mitigated by utilizing SCMs (i.e., blast furnace slag, fly ash, silica fume etc.) [19]. Hence, utilization of such by-products from manufacturing industries can mitigate the concrete reactivity concerns and thus advocate sustainability in current construction practice.

Ultra-high-performance concrete (UHPC) has recently emerged as an efficient alternative to normal strength concrete due to its superior mechanical and excellent durability characteristics, with high demand in infrastructures designed for long service life. According to some available literature, UHPC is a new generation concrete that possesses an ultra-high strength of at least 120 MPa [20, 21]. UHPC is defined by its relatively high binder content and significantly lower water-to-binder ratio compared to conventional concrete. Enhancement of microstructure, improvement of homogeneity, acceleration of hydration reactions, toughness improvement, and a significant reduction in porosity are the key manufacturing principles of UHPC [22, 23]. Uniform and dense microstructure and improved interfacial transition zone (ITZ) lead to the superior performance of UHPC compared to conventional concrete. Utilization of SCMs [22, 24] and use of water reducing superplasticizers particularly containing polycarboxylates [25] helps to achieve superior strength and maintain workability even though the water-to-binder ratio is kept relatively low. High binder content and use of superplasticizers in UHPC produces high heat during hydration and causes higher shrinkage strains, which is the prime reason behind its susceptibility to cracking [24, 26]. The portion of autogenous shrinkage is significantly larger in UHPC than

normal concrete due to the presence of high binder content and a very low water-to-binder ratio. Partial replacement of mixing water by crushed ice [27], applying heat curing [23], limiting the dosage of superplasticizer [26], and incorporation of super absorbent polymers [28], etc. are some innovative approaches to mitigate shrinkage in UHPC.

The above-mentioned papers on UHPC mainly dealt with concrete using fresh water and river sand. Natural and artificial seawater, as well as sea sand, have been successfully used in the preparation of ultra-high-performance concrete which achieved satisfactory mechanical characteristics [29]. In consideration of the review above, there is a lack of research on the strength, workability, and shrinkage of ultra-high-performance seawater and sea sand concrete (UHP-SWSSC), OPC-slag based UHP-SWSSC, let alone the influence of OPC replacement ratio on the strength, workability, and dimensional stability (e.g., volumetric change of concrete due to shrinkage). This paper explores the possibility to develop a UHP-SWSSC from local marine resources in Australia which utilize industrial by-products such as blast furnace slag and silica fume to replace OPC. Several mixes were prepared by varying the cement replacement ratio (0% as the control mix, 25%, 37.5%, 50%, and 62.5%), aggregate type, and water-to-binder ratio. The impact of these parameters on the compressive strength and workability was assessed. UHPC with a similar mixing ratio but utilizing tap water and river sand as well as washed Sydney beach sand were prepared and analyzed to compare with the seawater and sea sand UHPC. The influence of different types of aggregates, cement substitution ratio, and water-to-binder ratio on early age and long-term shrinkage properties of UHPC was determined. Finally, an appropriate UHP-SWSSC mix was selected based on its physical, mechanical, and dimensional stability characteristics.

2. Raw Materials, Mix Proportions, and Methods

2.1. Raw Materials

A general-purpose ordinary Portland cement conforming to AS 3972-2010 [30] was used in this study with two supplementary cementitious materials (SCMs) – ground granulated blast furnace slag (GGBFS) and undensified silica fume conforming to AS 3582.2-2016 [31] and AS/NZS 3582.3-2016 [32], respectively. The slag was sourced from Australian Steel Mill Services (ASMS), Port Kembla, NSW, and the silica fume was sourced from Simcoa, plant Kemerton, Western Australia. Chemical oxide compositions of the binders (**Table 1**) were determined by X-ray fluorescence (XRF) spectroscopy in an AXIOS WDXRF instrument and SUPERQ software was used for data analysis.

[Table 1 near here]

Natural seawater and sea sand were collected from Malabar beach of Sydney, NSW, Australia for fabricating UHPC. The cations and anions in seawater were detected through inductively coupled plasma – optical emission spectrometry (ICP-OES) and ion chromatography (IC), respectively. **Table 2** compares the ion concentrations of the natural seawater used in this study with that of the world average values [29]. The seawater collected from Malabar beach was found to be reasonably close to the corresponding world average values. Tap water was used in mixing and curing of tap water river sand and tap water washed Sydney beach sand UHPC.

[Table 2 near here]

[Figure 1 near here]

The sea sand was sieved through a 1.18 mm sieve to separate the stones, seashells, organic materials, and other impurities such as portions of aquatic plants, branches, man-made pollutants, etc., as per Willie and Boisvert-Cotulio [33] recommendations. The processed sand is presented in **Figure 1**. The total mass of impurities was 2.85% of the natural sea sand. Natural river sand was obtained from Taren Point, New South Wales. The washed beach sand was collected from beaches outside Sydney and washed thoroughly with fresh water to make it salt-free. Particle size distribution of different sands determined according to AS 1141.11.1-2009 [34] are compared in **Figure 2**. Sea sand with and without impurities is termed as 'sea sand before processing' and 'sea sand after processing', respectively. Natural river sand was found to be well graded, while the sea sand was gap graded with a significant portion of its particles retaining on 0.3 mm and 0.6 mm sieves. To avoid any effect of aggregate gradation in this study, natural river sand with the same particle size distribution as the sea sand was used. This modified river sand is termed as 'processed river sand' in this study. Modification of the sea sand by eliminating larger-sized particles does not alter its particle size distribution. The fineness of sea sand was found to be in between washed Sydney beach sand and natural river sand.

[Figure 2 near here]

The chemical composition of the sands was determined using the X-ray fluorescence (XRF) spectroscopy technique and presented in **Table 3**. It is evident that the sands are rich in silica. **Table 4** lists various physical properties of the sands used in this study including particle densities (i.e., oven-dry density, saturated surface dry or SSD density, apparent density), bulk densities (uncompacted and compacted), percentage of water absorption, and percentage void determined following relevant standards [35-37]. Natural river sand was found to possess slightly higher oven dry as well as SSD particle density compared to marine sands, due to the presence of a bigger

proportion of larger-sized aggregates (especially over 1.18 mm) in natural river sand and light-weight sea-shell fragments in sea sand. Water absorption of sea sand is the highest (3.46%), whereas natural river sand has the lowest water absorption (1.68%). Difference between the uncompacted and compacted bulk density was found to be higher in natural river sand, because of the presence of aggregates with various size ranges. Percent voids were measured to be very similar among different sand types (ranging between 39 – 41%).

The surface morphology of different sand particles and SCMs were assessed through SEM micrographs as shown in **Figure 3**. The procedure for microstructural analysis is discussed in **Section 2.3.3.**

[Figure 3 near here]

[Table 3 near here]

MasterGlenium SKY 8700, a polycarboxylate-based high range water reducer (HRWR) conforming to the requirements of AS 1478.1 [38], was used for batching UHP-SWSSC for its excellent cement dispersion and slump retention ability along with its suitability to be used with self-compacting concrete.

[Table 4 near here]

2.2. Mix Proportions, Batching, and Specimen Preparation

A total of 12 UHPC and one normal strength concrete mixes summarized in **Table 5** were investigated in this study. No steel fiber was added to the UHPC in order to produce an economically viable mix and eliminate the chances of steel corrosion. Seven UHPC mixes were prepared with seawater and sea sand (UHP-SWSSC), two from washed Sydney beach sand and

156 tap water (UHP-TWWBSC), and the remaining three utilized river sand and tap water (UHP-
157 TWRSC). Five mix ratios with varying proportions of OPC replacements were chosen for UHP-
158 SWSSC. UHP-SWSSCC with 100% OPC (termed as 'control mix') along with 25%, 37.5%, 50%,
159 and 62.5% of OPC replacement by ground slag and silica fume were produced. The control mix
160 was developed based on the recommendations provided by Willie and Boisvert-Cotulio [33] and
161 through a trial-and-error process until a suitable mix with satisfactory flowability and strength was
162 achieved. Although the ratio of OPC to supplemental material (ground slag in this study) is
163 suggested to be 1:0.25 by weight in [33], this study explores the possibility to utilize slag at a much
164 higher proportion (up to a ratio of OPC: slag = 1:1.33). In the OPC replaced mixes, the portion of
165 silica fume was kept constant at 12.5% of the total binder (except OPC-slag binary mix with 25%
166 substitution of OPC). Total binder content, aggregate content, water-to-binder ratio, and
167 superplasticizer-to-binder ratio were kept the same for all the mixes with different OPC
168 replacements (1200 kg/m^3, 1000 kg/m^3, 0.2, and 0.02, respectively). Two more seawater and sea
169 sand UHPC mixes were prepared by altering the water-to-binder ratio (0.15 and 0.25) of the 50%
170 OPC replaced mix. **Table 5** also presents the label for each of the concrete mixes (termed as 'mix
171 ID'); each label consists of the type of aggregate used, percentage of OPC replacement, and water-
172 to-binder ratio. For example, a mix ID of SS-50-0.2 refers to the UHPC mix where sea sand has
173 been used as aggregate, with an OPC substitution of 50% and a water-to-binder ratio of 0.2.

174 ***[Table 5 near here]***

175 For batching, the cement, SCMs and SSD fine aggregate were dry mixed for ten minutes at low
176 speed (50 rpm) in a laboratory pan mixer capable of controlling mixing speed. Water and HRWR
177 were mixed separately as per admixture supplier recommendations and later added to the dry
178 materials over 30 seconds. Afterward, mixing was continued for an additional 8 minutes at low

speed and another 2 minutes at medium speed (100 rpm) until a workable mix was attained. UHPC prepared in this study was found to be highly flowable and self-compacting, except for the mixes with significant OPC replacement and a very low water-to-binder ratio (particularly, SS-50-0.15). Immediately after mixing, the flow spread of the fresh UHPC was measured on a flow table as per ASTM C1437-15 [39] guidelines and the fresh density was measured following procedures outlined in ASTM C 138 [40]. According to the relevant standard [21], the flow table test was modified to adjust to UHPC's fluid nature. Concrete was poured into a mold in a single layer without tamping, the table was not dropped, and the fresh concrete was allowed to flow. The diameter of the flow spread was measured and reported. Simultaneously, standard 50 mm × 50 mm cube specimens were prepared and compacted on a vibrating table running at low frequency. The molds were then stored in a temperature and moisture-controlled cabinet at 23°C and relative humidity of 50% for 24 ± 2 hours. After the specified time, the concrete specimens were demoulded, and water cured. Two sets of specimens from each mix were prepared; one set was cured in a 23°C lime-saturated water bath while the other was cured in natural seawater at the same temperature. A set of 25 mm × 25 mm × 285 mm prisms were also prepared from each batch to monitor UHPC's shrinkage behavior.

2.3. Testing Procedures

2.3.1. Heat of hydration

The heat evolved in the first 72 hours of hydration of some representative UHPC pastes was captured in a TAM Air isothermal calorimeter operating at 23°C. From **Table 5**, the paste portion of SS-0-0.2, RS(P)-0-0.2, and SS-50-0.2 were chosen for the test to evaluate the effects of seawater and SCM on the reaction kinetics of UHPC. For this purpose, about 12 g paste sample was hand-mixed in a 20 ml glass ampoule and sealed before quickly transferring the specimen along with an

inert reference sample (oven-dried quartz sand) in the calorimeter chambers. Each reference sample mass was determined to have the same heat capacity as the UHPC paste sample. The time elapsed between the addition of the mix water and the start of the test was adjusted during data analysis. Each test was replicated to confirm the repeatability of the method.

2.3.2. Mechanical properties and shrinkage

For each mix proportion and curing condition studied, the 1, 3, 7, 28, and 90 days compressive strength of 50 mm × 50 mm cube specimens were determined following the requirements of ASTM C109/C109M-2020 [41]. Meanwhile, length change of prism specimens was measured up to an extended period of 120 days to determine the long-term drying and autogenous shrinkage of UHPC. The total shrinkage samples were air-dried after demoulding in a moist chamber at a constant conditioning temperature of 23°C and 50% relative humidity while the autogenous shrinkage samples were properly sealed with aluminum tape to prevent any loss of moisture and thus obtain their autogenous shrinkage at the same temperature and relative humidity. The total and autogenous shrinkages were determined by measuring the length change of the specimens according to AS 1012.13-2015 [42]. Drying shrinkage was determined from the difference between the respective total shrinkage and autogenous shrinkage.

2.3.3. Microscopic imaging

A Hitachi S3400 scanning electron microscope (SEM) was utilized for investigating the microstructure of 28 days mature UHPC. For this purpose, about 5 mm thick slices of samples were cut using a slow-rotating diamond saw. Specimens were immersed in 100% ethyl alcohol to stop the hydration and impurities were eliminated by ultrasonic cleansing. The imaging surface of the specimens was gold coated in an Emitech K550x gold sputter coater. For imaging raw binders and sands, the particles were attached on an adhesive carbon tape and gold coated. The accelerating

current for imaging was set at 30 amps with a beam strength of 20 kV and a working distance of approximately 5 mm under a high vacuum mode. Images of the microstructure were captured using the backscattered electron (BSE) mode of the electron microscope.

3. Results and Discussions

3.1. Heat of Hydration

The heat evolution in the first 72 hours of cement hydration (normalized per unit mass of cement) in the presence of tap water, seawater, and SCMs (slag and silica fume) is illustrated in **Figure 4**. The typical stages of cement hydration such as the dissolution of cement particles as identified in the initial peak right after the addition of water, induction peak, and the acceleration peak marking the hydration of cement [43] are observed in **Figure 4(a)**. The temporal change in the occurrence of the acceleration peak suggests that seawater accelerates cement hydration. The acceleration peak shifts by at least 6-8 hours from seawater hydration of cement along with reaching about 15% higher heat flow. A similar phenomenon is also observed when 50% cement is replaced by 37.5% slag and 12.5% silica fume. However, the mechanism behind them is different.

[Figure 4 near here]

When seawater is utilized in the mix, the abundance of chloride ions chemically binds with the calcium, aluminate, and ferrous phases of cement [44], forming insoluble calcium oxychloride phase and Friedel's salt [45]. When SCMs replace 50% of cement, it causes a similar effect, but from the well-explored filler effect [46, 47]. The slag and silica fume particles act as fillers between cement particles and offer extra nucleation sites for hydration products to occupy [46, 47]. As such, the heat evolved per unit mass of cement is higher than cement-only paste. This is also reflected in **Figure 4(b)** which shows a significantly higher cumulative heat generated per unit

mass of cement confirming the filler effect of SCMs. The heat of hydration of cement from seawater and tap water mixing after 72 hours of hydration is somewhat similar, but seawater mixing generates more heat in between 12-30 hours. Thus, it is expected that the 1-day strength of seawater composite could exceed that of tap water, however, may follow a similar strength development in later ages of hydration.

3.2. Properties of Fresh Concrete

The fresh and 28 days SSD density of UHPC are summarized in **Table 6**. The SSD density of concrete was found to be greater than its fresh density for all the mixes due to the continuing water absorption during the curing period. UHPC was found to possess around 6.6% greater unit weight than normal strength concrete because of its significantly compact microstructure from the selection of lower water-to-binder ratio [48]. The unit weight of seawater sea sand UHPC was found to be marginally higher than tap water river sand and washed beach sand UHPC, for both 100% OPC and 50% OPC replaced mix. However, when sea sand is replaced with washed beach sand and river sand, the fresh densities drop by 0.35% and 0.9%, respectively. The use of seawater may have resulted in the slight increase in density from the formation of more hydration products as captured in the heat evolution curves in **Figure 4**.

[Table 6 near here]

The incorporation of SCMs reduced the unit weight of UHPC, possibly due to the lower densities of SCM compared to OPC. The percentage of OPC replacement has been found to have a linear relationship with the decrease in a unit weight of both fresh and 28-day SSD unit weight. From **Table 6**, an OPC replacement of 25%, 37.5%, 50% and 62.5% yielded in a reduction of 1.15%, 3.49%, 3.99% and 4.01%, respectively in the unit weight of fresh UHP-SWSSC. The incorporation

of silica fume had a greater effect on unit weight reduction compared to ground slag, due to the significantly lower relative density of silica fume than cement and slag used in this study. These findings are consistent with previous studies of Zain et al. [48] and Turk [49].

The UHPC mixes reported in **Table 5** were trialed to possess excellent workability in general; their flow spread is summarized in **Figure 5**. The high flowability was achieved due to the utilization of polycarboxylate-based superplasticizer at a relatively high dosage than recommended for normal grade concrete. Regardless, the effects of slag, silica fume, and the use of different types of sand on the flowability can still be comparatively assessed. In general, the presence of ground slag decreased the flowability of all UHPC mixes. For instance, a 12.5% reduction in the flow spread resulted from the 25% replacement of cement with slag (**Figure 5(a)**). The angular shape of slag particles (shown in **Figure 3(d)**) together with the accelerated calcium reaction is possibly the primary reason behind the reduced flowability. However, the workability of UHPC improved when silica fume was added in addition to slag as partial replacements of OPC. The ternary blends produced better workability compared to the OPC-slag binary blend from the 'ball bearing' and lubricating effect of the spherical silica fume particles, as demonstrated in **Figure 3(e)** [50-52]. The addition of 12.5% silica fume in SS-37.5-0.2 increased the flow spread by 12.7% compared to the OPC-slag binary mix. However, with the increase of slag content in ternary blends, the flow degraded. The SS-62.5-0.2 mix with 50% ground slag and 12.5% silica fume yielded a 19.4% lower flow spread compared to the control mix. This particular mix was viscous and required high-frequency vibration for proper compaction.

[Figure 5 near here]

From **Figure 5(b)**, the flowability of UHPC slightly declined from the use of sea sand and seawater. The uniformity and size fractions of sea sand particles together with the presence of irregularly shaped seashells and other micro-impurities may have led to a reduced flow [2]. **Figure 3** confirms that washed beach sand particles are round in shape with a relatively smooth surface, while the river sand particles are mostly angular with rough edges and varying size fractions. The angularity and roughness of sea sand somewhat lie in between the washed beach sand and river sand, which is also reflected in the flowability of UHPC ranging in the same order. It is evident from **Figure 5(b)** that the control UHP-SWSSC mix had a flow spread of 360 mm, in contrast to 390 mm and 345 mm for washed Sydney beach sand and processed river sand UHPC with identical mix proportions. The 50% OPC replaced mixes also showed a similar trend.

In addition, the flow spread increased with the increase in the water-to-binder ratio, as expected (**Figure 5(c)**). 50% OPC replaced UHP-SWSSC with a water-to-binder ratio of 0.15, 0.2, and 0.25 produced slump spreads of 185 mm, 340 mm, and 360 mm, respectively. The SS-50-0.15 mix was found to be highly viscous, and the workability was challenged in specimen making; this also yielded a 45.6% reduced spread compared to the SS-50-0.2. Chen et al. [53] reported that UHPC's extremely low water content is insufficient to fill the inter-particular void spaces and is readily absorbed around the particle surfaces while leaving the voids empty. This study found a water-to-binder ratio of 0.2 to be optimum for lubrication of the granular materials at a superplasticizer dose of 24 kg/m^3. Overall, the workability of all the UHPC mixes in this study was found to be similar in comparison with the targeted 280 mm – 340 mm flow spread of Willie and Boisvert-Cotulio [33]. The results are also consistent with the flowability of seawater and sea sand UHPC studied by Teng et al. [29].

3.3. Compressive Strength

Table 7 summarizes the compressive strength of all mixes investigated in this study under both tap water and seawater curing regimes; the results are the mean of the strength of three identical specimens. The strength of conventional concrete cylinders under tap water curing was also assessed for comparison purposes. The 1-day strength was determined just after demoulding of specimens and before storing them in the curing chamber. The standard deviation is well within 5% of the compressive strength value, which indicates lesser variability and better homogeneity of respective UHPC mixes. The following section highlights the influence of several mix proportion parameters on the compressive strength of UHPC.

[Table 7 near here]

3.3.1. Effect of seawater and sea sand

Figure 6 shows the comparative compressive strength development of UHPC composed of different types of sand and mixing water under tap water curing conditions. The incorporation of sea sand and seawater in UHPC can produce relatively higher compressive strength at an early age, particularly, up to 28 days. The control mix SS-0-0.2 in this testing regime yielded substantially high early-age strength, with no cement replacement. However, comparative discussion can be made for the other mixes in which, the sand type is the only variable. Among the 50% OPC substituted mixes, the seawater and sea sand mix (SS-50-0.2) produces 29.1%, 16.8%, and 13.9% larger compressive strength values in comparison with tap water and washed beach sand mix after 1, 3, and 7 days, respectively. Although in the early ages, the difference is more pronounced, the long-term (90 days) strength of all mixes is similar. The seawater and sea sand mix reached 62.5% of its 90-day strength at an age of only 3 days, whereas the river sand and washed beach sand mixes utilizing tap water in mixing achieved slightly over half of their long-

term strength at three days. This indicates that seawater accelerates the hydration of the binder, providing early-age strength gain to UHPC. This is also reflected in the heat of hydration curves in **Figure 4** which shows greater heat release from the use of seawater. For tap water mixing, the hydration continues beyond 28 days, although at a slower pace, but reaches a similar strength as that of seawater mixed UHPC. The higher early-age compressive strength is due to the abundance of chloride content in sea sand and seawater which accelerates the hydration reaction initially. Faster hydration generates a greater amount of hydration products, such as calcium silicate hydrate (C-S-H), which blocks the pores in the resulting concrete and thus enhances the early strength development [2, 16].

[Figure 6 near here]

However, the development of strength gain in UHP-SWSSC slows down with time, especially after 28 days. The UHP-SWSSC mix with 50% cement substitution (SS-50-0.2) yields the highest strength of 136.8 MPa after 28 days of tap water curing, which is a mere increase (6% and 2.2%, respectively) compared to UHP-TWWBSC and UHP-TWRSC counterparts. Similar trends were also observed when mixes were cured in a seawater environment. This deterioration in strength gain occurs as a result of leaching out of soft hydration products with time [11, 14]. Long-term strengths, especially after 90 days of curing were found to be almost identical, which aligns with the findings of the studies of Mohammed et al. [12]. Overall, a slight increase in the early age strength and a slight reduction in the long-term strength of SCM-based UHP-SWSSC were consistent with the results of Teng et al. [29].

355 *3.3.2. Effect of OPC replacement by ground slag and silica fume*

356 It is apparent from **Figure 7** that in general, UHPCs produce significantly higher strength (about
357 4 times) than normal strength concrete with a water-to-binder ratio of 0.35. The ratio of strength
358 between OPC-based UHPC and NC was found to be higher at an early age (a strength ratio of 4.7
359 after 1-day), whereas a slightly reduced strength ratio of 3.4 has been found for long-term 90-day
360 compressive strength. This indicates the faster development of strength in UHPC with high binder
361 content at a significantly lower water-to-binder ratio.

362 ***[Figure 7 near here]***

363 It has been found that early-age strength decreases with the increase in OPC replacement. UHPC
364 with no cement replacement yielded a compressive strength of 85.2 MPa at day 1, whereas 25%,
365 37.5%, 50%, and 62.5% OPC replaced mixes produced respectively 57 MPa, 38.9 MPa, 37.3 MPa,
366 and 22.9 MPa strength at the same age. OPC substitution by SCMs, such as silica fume and ground
367 slag, was found to yield lower strength initially, up to as early as 7 days of casting. The slower rate
368 of pozzolanic reaction of ground granulated blast furnace slag at room temperature curing hinders
369 the early age strength development [54]. However, OPC substituted mixes tend to generate more
370 strength compared to cement-based mixes as time goes on, especially after 28 days of curing and
371 beyond. In our study, 28-days, as well as 90-days strengths of all UHP-SWSSC mixes, were found
372 to be quite similar, with a slight increase of strength for higher OPC replacements. For example,
373 the 50% OPC replaced mix reaches a compressive strength of 136.8 MPa after 28 days of tap water
374 curing, while the 100% OPC variant has a slightly lower strength of 127.4 MPa. The strength ratios
375 of 62.5% cement replaced mix to control mix were 0.27, 0.71, 0.95, 1.03, and 1.05 after tap water
376 curing periods of 1, 3, 7, 28, and 90 days correspondingly. The short-term strengths were
377 considerably lower in comparison with the control mix, while slightly higher long-term strengths

were observed. Silica fume with significantly smaller particle size has a filler effect which improves the particle packing density. The highly pozzolanic slag and silica fume convert the $Ca(OH)_2$ into secondary C-S-H and thus enhance the interfacial bond, which eventually leads to more homogeneous ITZ and therefore, an increased strength [54, 55]. Overall improvement of microstructure in SCM incorporated UHPC blends enables them to achieve higher strength compared to OPC based UHPC.

[Figure 8 near here]

UHP-SWSSC mixes with different proportions of cement replacement show identical trends when cured under a seawater environment (**Figure 8).** The mix with 50% OPC replacement yields 56.3% and 24.9% lower strength after 1 and 3 days of curing compared to the control mix, however it generates 10.8% and 7.5% higher strength after a curing period of 28 and 90 days, respectively.

3.3.3. Effect of water-to-binder ratio

Three mixes of 50% cement replaced UHP-SWSSC were compared with varying water-to-binder ratios, i.e., 0.15, 0.2, and 0.25. In general, an increase in the water-to-binder ratio causes a reduction in compressive strength (**Figure 9**). This result is consistent with the findings of Zhang and Zhang [56], where it was found that the reduction of water content in the UHPC matrix densifies the hydration film produced around the surface of cementitious particles, which prohibits further hydration reaction. Additionally, lowering the water-to-binder ratio reduces the porosity in microstructure, which eventually leads to greater strength. However, early age strength was seen to be impacted more compared to long-term strength. Increasing the water-to-binder ratio from 0.15 to 0.25 reduces the 1-day and 3-days strength by 59.8% and 20.2%, whereas the strength reductions were found to be 6.4% and 3.5% after 28 and 90 days, respectively.

[Figure 9 near here]

Interestingly, the SS-50-0.2 mix with a water-to-binder ratio of 0.2 yielded marginally higher 28-day strength compared to the counterpart SS-50-0.15 with a lower water-to-binder ratio. In the case of extremely low water content, the available water is completely absorbed within the particle surfaces, thereby leaving the voids empty. If the water content in the cementitious matrix is lower than a minimum margin, the strength does not increase due to the void spaces present in the microstructure and due to the unavailability of water for hydration of cement particles [53, 56]. The UHPC mix with a very low water-to-binder ratio of 0.15 was found to be sticky and viscous, with a flow spread of only 185 mm (**Figure 5(c)**). The cross-section exhibited visible air voids as shown in **Figure 10(a),** which could not be eliminated through vibration. The porous microstructure with an extremely low water-to-binder ratio inhibits its ability to gain long-term ultra-high strength. In contrast, cross-sections of SS-50-0.2 and SS-50-0.25 mixes were more homogeneous with almost no visible air voids, as shown in **Figure 10(b)** and **Figure 10(c)**. The optimum water-to-binder ratio in order to achieve maximum long-term compressive strength was found to be 0.2.

[Figure 10 near here]

3.3.4. Effect of curing condition

The influence of seawater curing on the compressive strength of UHPC comprised of different aggregates is depicted in **Figure 11** and **Figure 12**. Overall, seawater incorporated as curing water has a negative impact on the strength of UHPC. The 100% OPC-based UHP-SWSSC samples cured in tap water yielded higher strength compared to curing in seawater, 3.3%, 8.8%, 13.5%, and 13.8% strength enhancement after curing periods of 3, 7, 28, and 90 days, respectively

(**Figure 11**). River sand and washed Sydney beach sand-based UHPC experienced similar deterioration in strength while cured in seawater, with 8.67% and 9.31% of reduction, respectively after a prolonged seawater curing period of 90 days. The loss of strength in seawater-cured cement-based UHPC has been observed to escalate with the curing age. The degradation of strength gain may have occurred because of the formation of expansive (such as ettringite and Friedel's salt) as well as soft leachable compounds in the cementitious microstructure due to seawater penetration during prolonged exposure [14]. Development of micro-cracks due to chloride and sulfate attacks from harsh seawater environments as well as salt crystallization is known to occur in concrete with high cement contents [57]. The combined phenomena explain the deterioration of long-term strength development of UHPC under seawater curing regime.

[Figure 11 near here]

Similar behavior has been observed in SCM-based UHP-SWSSC. In comparison with seawater curing, 50% OPC replaced UHP-SWSSC mixes attain a compressive strength increase of 18.5%, 9.6%, 10%, and 9.7% respectively after the age of 3, 7, 28, and 90 days in tap water curing (**Figure 12**). Contrary to OPC-based UHPC, early age strength is more impacted than long-term strength in slag and silica fume-based UHPC, regardless of the sand type utilized. The addition of SCMs furthers the hydration reaction due to their enhanced pozzolanic activity, which continues to densify the microstructure as time progresses. Therefore, SCM-based UHPC experiences lower compressive strength loss under a harsh seawater environment [58].

[Figure 12 near here]

3.4. Shrinkage

3.4.1. Effect of sand type

Figure 13 compares the total, autogenous, and drying shrinkage of UHPC comprising of three different types of sand and that of conventional concrete. UHPCs experienced significantly higher autogenous shrinkage, and therefore higher total shrinkage compared to normal concrete (**Figure 13 (a, b)**). The 7 day early-age and 120 day long-term autogenous shrinkage of UHP-SWSSC was found to be 15 and 6 times larger than that of normal concrete, respectively. As the negligible water content in UHPC is not enough for complete hydration of binder contents, greater surface tension is created in the fine capillary pores of the cementitious matrix, which leads to larger autogenous shrinkage [23, 59]. UHPC experiences a very quick self-desiccation during the first few days after casting and thus obtains a very high early autogenous strain rate. The early growth (first 7 days) of autogenous shrinkage is slower in plain concrete. While normal concrete reaches only 28% of its maximum autogenous shrinkage gained over 120 days testing period, UHP-SWSSC reaches 72% of its maximum autogenous shrinkage in the same duration (**Figure 14**). It can be observed from **Figure 15** that the proportion of autogenous shrinkage is insignificant in NC (< 20% of total shrinkage) but it is significant in UHPC (over 40% in UHP-SWSSC and over 60% in UHP-TWRSC as well as UHP-TWWBSC).

[Figure 13 near here]

UHPC manufactured from seawater and sea sand in this study yielded considerably higher drying shrinkage strain than tap water and river sand or washed beach sand counterparts (**Figure 13(c)**), whereas the autogenous shrinkages were quite similar (**Figure 13(b)**). After 120 days of testing period, the drying shrinkage of UHP-SWSSC was 973.7 με, compared to 288 με and 347.3 με for UHP-TWWBSC and UHP-TWRSC respectively. Due to the presence of excessive sodium and

calcium chloride in seawater sea sand concrete, the morphology of the pore structure densifies, which increased the number of micropores. This eventually increases the capillary tension and therefore generates substantially high drying shrinkage [60, 61]. Additionally, the presence of sea-shell contents may have accounted for larger drying shrinkage in sea sand-based concrete, particularly due to the lower rigidity of sea-shell particles [62].

Although autogenous shrinkage dominates the total shrinkage in washed beach sand and river sand UHPC mixes (with a ratio of 120 days autogenous to drying shrinkage to be 2.23 and 1.89, respectively), the drying shrinkage strain component was observed to be larger in the seawater sea sand variant (ratio of autogenous to drying shrinkage was 0.7). Over the whole testing timeframe, autogenous shrinkage was less prominent in UHP-SWSSC (around 40-45% of the total shrinkage), whereas it formulated the major portion of the total shrinkage in river sand and washed beach sand UHPC (around 65-70%). It is evident from **Figure 14** that sea sand-based UHPC achieves 93% of its maximum autogenous shrinkage after 28 days from casting, whereas washed beach sand and river sand UHPCs reach respectively 75% and 73% at the same point of time. The increased amount of calcium chloride as a result of reactions between sodium chloride and calcium hydroxide in the pore solution of seawater-based UHPC is the prime reason behind its accelerated hydration [63]. Autogenous shrinkage strain in UHP-SWSSC reaches a plateau after 21 days indicating the completion of accelerated hydration, whereas it takes around 100 days to stabilize in UHP-TWRSC and UHP-TWWBSC. Therefore, UHP-SWSSC may be susceptible to early-age cracking due to its high early-age autogenous shrinkage.

[Figure 14 near here]

Overall, the growth of drying shrinkage in UHP-SWSSC is slower than river sand and washed beach sand UHPCs. Drying shrinkage strain in UHP-SWSSC stabilizes after 84 days of casting, while UHP-TWRSC and UHP-TWWBSC take only around 21 days to attain plateau. Very small pores in the compact microstructure of UHP-SWSSC continue their capillary actions for an extended time, which leads to the gradual increase of the drying shrinkage.

[Figure 15 near here]

3.4.2. Effect of SCMs

It was observed from **Figure 16(a)** that replacement of OPC by SCMs tends to decrease the overall shrinkage of seawater and sea sand-based UHPC. Although the autogenous shrinkage was found to moderately increase **(Figure 16(b))**, the drying shrinkage considerably reduced when OPC was partially replaced by slag and silica fume **(Figure 16(c))**.

[Figure 16 near here]

A more detailed comparison on the growth of autogenous shrinkage suggests that the autogenous shrinkage in OPC-slag-silica fume trinary mix was lower than OPC-slag binary mix. However, both types of mixes yielded greater autogenous shrinkage compared to cement-only UHPC. Incorporation of slag and silica fume is known to enhance the autogenous shrinkage of concrete due to their ability to refine the microstructure into a finer pore capillary system, which increases the degree of self-desiccation, leading to a higher autogenous shrinkage [64, 65]. Generally, the effect of silica fume in hydration is much more pronounced in fresh water-based UHPC compared to that of slag, especially at early ages. However, due to the alkaline environment and presence of a high quantity of sulfates in the pore solution of seawater mixed UHPC matrix, the hydration reaction of slag accelerates and the reactivity of silica fume with cement reduces [63]. The rapid

dissolution of slag and decelerated influence of silica fume in the hydration kinetics of UHP-SWSSC explains the larger autogenous shrinkage of OPC-slag UHPC compared to OPC-slag-silica fume ternary blends. However, as the slag content in ternary mixes increased, the autogenous shrinkage values also increased. After 120 days, the binary (25% OPC substitution by only slag) and ternary (37.5% OPC replacement by 25% slag and 12.5% silica fume) mixes yielded 50.9% and 6.7% higher autogenous shrinkage, respectively compared to the control mix. Blast furnace slag in UHP-SWSSC significantly elevates autogenous shrinkage, while further addition of silica fume balances this surge. **Figure 17** demonstrates the SEM images of shrinkage cracks in the microstructure of control UHP-SWSSC (**Figure 17(a)**) and the blend with 25% OPC replaced by slag (**Figure 17(b)**)**.** As the samples right after casting were sealed in closed plastic tubes and remained sealed until the day of SEM analysis, the shrinkage that occurred in the specimens was primarily autogenous shrinkage. A prominent network of autogenous shrinkage cracks was seen in the microstructure of 25% OPC replaced UHPC compared to UHPC with 100% OPC, where autogenous shrinkage cracks were almost nonexistent.

[Figure 17 near here]

The inclusion of slag and silica fume accelerates the growth of autogenous shrinkage development as well. This is from the higher degree of reaction of cement from the addition of SCMs as captured in the heat evolved per gram of cement (shown in **Figure 4**). In the control mix, drying shrinkage grows more rapidly than autogenous shrinkage (88% of drying and 50% of autogenous shrinkage develops in the first 7 days, as demonstrated in **Figure 18**). However, with more portion of OPC being replaced by slag and silica fume, autogenous shrinkage starts to grow quicker at early ages due to elevated interaction of slag in the cement-slag-silica fume ternary blends. For a 50%, OPC

replaced mix, 72% autogenous shrinkage develops after 7 days as opposed to 68% drying shrinkage.

[Figure 18 near here]

In general, the percentage of autogenous shrinkage with respect to total shrinkage increases with an increase in OPC replacement percentage. This applies especially to the OPC-slag binary mix, where autogenous shrinkage was 53% of the total shrinkage at 120 days, compared to 33% in the control mix (**Figure 19**). OPC replaced by only slag (or high content of slag) produces a high value of autogenous to drying shrinkage ratio. For instance, a 25% substitution of OPC by slag yielded an autogenous to drying shrinkage ratio of 1.14, compared to 0.49 for the control mix. Autogenous shrinkage was most significant in SS-62.5-0.2 (50% slag and 12.5% silica fume) as a result of its high slag inclusion (autogenous to drying shrinkage ratio of 1.28).

Drying shrinkage decrease with the increase of cement substitution by slag and silica fume unlike autogenous shrinkage, which is consistent with relevant literature [66]. This is attributed to the relatively denser microstructure in slag-based UHPC. A compact matrix contains lesser microstructural pores, which keeps water loss due to evaporation to a minimum and therefore leads to a decreased drying shrinkage. It was also noticed that drying shrinkage in silica fume added mixes grew slower than control and OPC-slag binary mixes. After 7 days of casting, the SS-62.5-0.2 ternary mix develops 72% of its ultimate drying shrinkage, compared to 88% and 94% growth in control and 25% slag replaced mixes, respectively (**Figure 18**). This delayed growth of drying shrinkage is probably because silica fume further densifies OPC-slag binary system and yields a more compact microstructure. In general, drying shrinkage becomes less prominent with more percentage of OPC supplanted by slag and silica fume.

[Figure 19 near here]

3.4.3. Effect of water-to-binder ratio

Figure 20 illustrates the effect of the water-to-binder ratio on the shrinkage of UHP-SWSSC. From **Figure 20(c)**, it is observed that the drying shrinkage in the UHPC with higher water content is larger than the lower water-to-binder ratio counterparts (701.6 με in SS-0.50-0.15 compared to 1090 με in SS-50-0.25 after 120 days of casting). More pores are formed in a concrete mix with larger water content, which produces higher surface tension in the pore structure during evaporation [26].

[Figure 20 near here]

Several literatures have reported an increase in autogenous shrinkage with the reduction of water-to-cement ratio in high-performance concrete [59], ultra-high performance concrete [64], and reactive powder concrete [26] as a result of enhanced internal drying, self-desiccation, and capillary tension. However, a quite opposite finding has been obtained in this research regarding seawater and sea sand-based UHPCs. From **Figure 20 (b)**, the autogenous shrinkage was observed to increase with the increase in the water-to-binder ratio of UHP-SWSSC. Autogenous shrinkage grew faster when the water-to-binder ratio was higher, especially at early ages, which may have occurred due to the effect of seawater on the ternary blend of OPC, slag, and silica fume. For example, 69% and 80% of maximum autogenous shrinkage were reached in the first 7 days for mixes with the water-to-binder ratio of 0.15 and 0.25, respectively (**Figure 21**). As discussed in **Section 3.4.2**, the incorporation of seawater in pastes with a low water-to-binder ratio can increase the reactivity of slag, especially at early ages [63]. A higher amount of seawater-induced ions and higher alkalinity in mixes with larger water content can accelerate the hydration rate of slag to a

greater extent, which means enhanced self-desiccation and greater autogenous shrinkage. This mechanism also explains the rapid initiation of autogenous shrinkage in higher water-to-binder ratio mixes. It is evident from **Figure 21** that the development of autogenous shrinkage is lower than drying shrinkage during the first 7 days in the SS-50-0.15 mix. However, for SS-50-0.25 mix with higher water content, growth of autogenous shrinkage after 7 and 28 days was significantly higher than drying shrinkage. No clear trend regarding the proportions of autogenous and drying shrinkage was obtained in mixes with different water-to-binder ratios (**Figure 22**).

[Figure 21 near here]

Although autogenous shrinkage usually governs the overall shrinkage in reactive powder concrete, overall drying shrinkage was found to be dominant in seawater and sea sand-based UHPC in this study, with a couple of exceptions of OPC-slag binary mix (SS-25-0.2) and a large portion of slag incorporated ternary mix (SS-62.5-0.2). The relatively lower proportion of autogenous shrinkage in UHP-SWSSC is advantageous particularly in terms of early-age autogenous shrinkage-induced cracking.

[Figure 22 near here]

4. Selection of a Proper Mix based on Physical, Mechanical and Dimensional Stability Properties

Physical, mechanical, and dimensional stability properties of the industrial by-product based seawater and sea sand UHPC mixes are compared in **Table 8** to evaluate their performance. Properties of the individual mixes were compared against the control mix (SS-0-0.2). An increase or a decrease in the properties with respect to the control mix has been quantified by a positive or negative percentage, respectively. It is evident from the comparison that the OPC replaced UHP-

SWSSC mixes possessed slightly lower fresh as well as 28-day unit weight. Workability of UHP-SWSSC can be an issue if a high proportion of slag is added (>37.5% of the total binder) or the water-to-binder ratio is kept relatively low (<0.2). Although early age compressive strengths were smaller than the control mix, strength increased with time and exceeded the control mix after 90 days. Overall, autogenous shrinkage was higher (except SS-50-0.15) and drying shrinkage was lower with respect to the control mix. When added together, total shrinkage was also lower compared to the control mix (except SS-50-0.25). Comparing the mechanical and dimensional stability properties, the SS-50-0.2 mix is recommended in this study. Compared to the control mix, this mix achieved slightly higher long-term strength (7.47%) and lower total shrinkage strain (10.95%) without compromising the workability. Although a marginal reduction in workability (5.56%) and a moderate increase in the autogenous shrinkage (15.92%) was observed, this blend yielded satisfactory performance among other UHP-SWSSC mixes with different OPC substitution percentages and water-to-binder ratios.

XRF analysis of ground concrete powder reveals the chloride content of mature UHPC samples. Most importantly, the chloride content of the seawater and sea sand UHPC mix was determined to be 8.0 kg/m^3, as opposed to 0.72 kg/m^3 for tap water and river sand-based UHPC. Chloride content found in UHP-SWSSC was found to be 10 times higher than the AS 1379 [67] limits of 0.8 kg/m^3 for normal class concrete. However, the experimental results of this study provide evidence that marine resources can still be utilized in UHPC fabrication for unreinforced applications or may be embedded with corrosion-resistant reinforcement, such as FRPs. The durability study of seawater and sea sand UHPC mixes which is currently underway by this research group will provide critical data for a well-informed cost-benefit-sustainability analysis.

[Table 8 near here]

5. Conclusions

The following conclusions can be drawn within the limited scope of this preliminary study on the potential of using seawater and sea sand in UHPC fabrication:

- Seawater accelerates cement hydration and releases more heat from the formation of Friedel's salt in the early ages of hydration. This is also reflected in the early-age compressive strength.
- Incorporation of seawater and sea sand in UHPC yields marginally higher fresh and hardened density compared to river sand and washed beach sand counterparts, whereas industrial by-products such as ground slag and silica fume reduce the unit weight of UHP-SWSSC.
- The use of sea sand and seawater in UHPC slightly decreases its workability. However, silica fume in an OPC-slag-silica fume ternary blend offers better workability compared to OPC-slag binary blends. A sufficiently workable mix at a water-to-binder ratio of 0.2 can be achieved under an optimized superplasticizer dose with a maximum 50% OPC replacement with SCMs.
- Sea sand and seawater UHPCs provide a higher rate of strength development especially up to 28 days, beyond which, the strength development slows down to reach similar 90 days strength. Slag and silica fume offer a similar 90 days strength from the delayed secondary hydration products from their pozzolanic reactivity. The optimum water-to-binder ratio to achieve maximum long-term compressive strength was found to be 0.2.
- Seawater curing lowers the long-term strength of OPC-based UHPC and the early age strength of SCM incorporated UHPC. However, UHPC with SCMs experiences marginal deterioration under seawater environment compared to cement-only counterpart.
- UHP-SWSSC produces high early-age autogenous shrinkage and considerably higher drying shrinkage than tap water and river sand or washed beach sand variants because of the

accelerated hydration of cement. SCM incorporation in the mix also increases autogenous shrinkage from the accelerated hydration of cement particles, but significantly reduces drying shrinkage from densifying the UHPC matrix, and hence reduces the overall shrinkage.

- A UHP-SWSSC mix with 50% OPC replaced by 37.5% slag and 12.5% silica fume is recommended in this study, which can achieve satisfactory workability, long-term strength, and dimensional stability properties.

Acknowledgments

This study has been funded by the Australian Research Council (ARC) through an ARC Discovery Grant (DP160100739). The authors wish to acknowledge Randwick Council for their permission to collect seawater and sea sand from Malabar beach in Sydney, NSW. We thank Mr. William Terry and Mr. Luiz Pettersen, technical staff of the Infrastructure Laboratory at UNSW for their assistance in the preparation of specimens. Finally, the authors also acknowledge the use of facilities within the Mark Wainwright Analytical Centre at UNSW for X-ray fluorescence spectroscopy and scanning electron microscopy.

References

1. *https://www.statista.com/statistics/1087115/global-cement-production-volume/ (accessed on 08.12.2021).*
2. Xiao J, Qiang C, Nanni A, et al., Use of sea-sand and seawater in concrete construction: Current status and future opportunities. *Construction and Building Materials*, 2017. **155**: p. 1101-1111.
3. Ercikdi B, Cihangir F, Kesimal A, et al., Utilization of industrial waste products as pozzolanic material in cemented paste backfill of high sulphide mill tailings. *Journal of Hazardous Materials*, 2009. **168**(2): p. 848-856.

4. Kumar R, Samanta AK and Roy DKS, Characterization and development of eco-friendly concrete using industrial waste - a review. *Journal of Urban and Environmental Engineering*, 2014. **8**(1): p. 98-108.
5. Teng J, Yu T, Dai J, et al. *FRP composites in new construction: current status and opportunities*. in *Proceedings of 7th National Conference on FRP Composites in Infrastructure (Supplementary Issue of Industrial Construction), keynote presentation, Hangzhou, China*. 2011.
6. Li YL, Zhao XL, Singh RKR, et al., Experimental study on seawater and sea sand concrete filled GFRP and stainless steel tubular stub columns. *Thin-Walled Structures*, 2016. **106**: p. 390-406.
7. Wang Z, Zhao X-L, Xian G, et al., Long-term durability of basalt- and glass-fibre reinforced polymer (BFRP/GFRP) bars in seawater and sea sand concrete environment. *Construction and Building Materials*, 2017. **139**: p. 467-489.
8. Dong Z-Q, Wu G, Zhao X-L, et al., Long-Term Bond Durability of Fiber-Reinforced Polymer Bars Embedded in Seawater Sea-Sand Concrete under Ocean Environments. 2018. **22**(5): p. 04018042.
9. Zeng J-J, Gao W-Y, Duan Z-J, et al., Axial compressive behavior of polyethylene terephthalate/carbon FRP-confined seawater sea-sand concrete in circular columns. *Construction and Building Materials*, 2020. **234**: p. 117383.
10. Ramaswamy S, Aziz M and Murthy C, *Sea dredged sand for concrete*, in *Extending Aggregate Resources*. 1982, ASTM International.
11. Kaushik SK and Islam S, Suitability of sea water for mixing structural concrete exposed to a marine environment. *Cement and Concrete Composites*, 1995. **17**(3): p. 177-185.
12. Mohammed TU, Hamada H and Yamaji T, Performance of seawater-mixed concrete in the tidal environment. *Cement and Concrete Research*, 2004. **34**(4): p. 593-601.
13. Etxeberria M, Fernandez JM and Limeira J, Secondary aggregates and seawater employment for sustainable concrete dyke blocks production: Case study. *Construction and Building Materials*, 2016. **113**: p. 586-595.
14. Islam MM, Islam MS, Al-Amin M, et al., Suitability of sea water on curing and compressive strength of structural concrete. *Journal of Civil Engineering (IEB)*, 2012. **40**(1): p. 37-45.

15. Cui M, Mao J-Z, Jia D-G, et al. *Experimental study on mechanical properties of marine sand and seawater concrete*. in *Proceedings of the 2014 International Conference on Mechanics and Civil Engineering*. 2014.
16. Limeira J, Agulló L and Etxeberria M, Dredged marine sand as a new source for construction materials. *Materiales de Construcción*, 2012. **62**(305): p. 7-24.
17. Modupeola AG and Olutoge FA, The effect of seawater on shrinkage properties of concrete. *Int J Res Eng Technol*, 2014. **2**(10): p. 1-12.
18. Younis A, Ebead U, Suraneni P, et al. *Strength, shrinkage, and permeability performance of seawater concrete*. in *10th International Structural Engineering and Construction Conference, ISEC 2019*. 2019. ISEC Press.
19. Mahanama D, Silva PD, Kim T, et al., Evaluating Effect of GGBFS in Alkali Silica Reaction in Geopolymer Mortar with Accelerated Mortar Bar Test. *ASCE Journal of Materials in Civil Engineering*, 2019. **31**(8): p. 04019167.
20. Balázs GLE, *Structural concrete: textbook on behaviour, design and performance. 1*. 2009: International Federation for Structural Concrete.
21. ASTM C1856 / C1856M–17 Standard practice for fabricating and testing specimens of ultra-high performance concrete. 2017, ASTM International: West Conshohocken.
22. Shi C, Wu Z, Xiao J, et al., A review on ultra high performance concrete: Part I. Raw materials and mixture design. *Construction and Building Materials*, 2015. **101**: p. 741-751.
23. Mishra O and Singh SP, An overview of microstructural and material properties of ultra-high-performance concrete. *Journal of Sustainable Cement-Based Materials*, 2019. **8**(2): p. 97-143.
24. Wang D, Shi C, Wu Z, et al., A review on ultra high performance concrete: Part II. Hydration, microstructure and properties. *Construction and Building Materials*, 2015. **96**: p. 368-377.
25. Schröfl C, Gruber M and Plank J, Preferential adsorption of polycarboxylate superplasticizers on cement and silica fume in ultra-high performance concrete (UHPC). *Cement and Concrete Research*, 2012. **42**(11): p. 1401-1408.
26. Tam CM, Tam VWY and Ng KM, Assessing drying shrinkage and water permeability of reactive powder concrete produced in Hong Kong. *Construction and Building Materials*, 2012. **26**(1): p. 79-89.

27. Xie T, Fang C, Mohamad Ali MS, et al., Characterizations of autogenous and drying shrinkage of ultra-high performance concrete (UHPC): An experimental study. *Cement and Concrete Composites*, 2018. **91**: p. 156-173.
28. Han J, Fang H and Wang K, Design and control shrinkage behavior of high-strength self-consolidating concrete using shrinkage-reducing admixture and super-absorbent polymer. *Journal of Sustainable Cement-Based Materials*, 2014. **3**(3-4): p. 182-190.
29. Teng J-G, Xiang Y, Yu T, et al., Development and mechanical behaviour of ultra-high-performance seawater sea-sand concrete. 2019. **22**(14): p. 3100-3120.
30. AS 3972 General purpose and blended cements. 2010, Standards-Australia.
31. AS 3582.2 Supplementary cementitious materials for use with portland and blended cement Slag - Ground granulated iron blast-furnace. 2016, Standards Australia.
32. AS/NZS 3582.3-2002 Supplementary cementitious materials for use with portland and blended cement - Amorphous silica. 2002, Standards-Australia.
33. Wille K and Boisvert-Cotulio C, Material efficiency in the design of ultra-high performance concrete. *Construction and Building Materials*, 2015. **86**: p. 33-43.
34. AS 1141.11.1 Methods for sampling and testing aggregates Particle size distribution - Sieving method. 2009, Standards Australia.
35. AS 1141.5 Methods for sampling and testing aggregates—particle density and water absorption of fine aggregate. 2000, Standards-Australia.
36. AS 1141.4-2000 Methods for sampling and testing aggregates, Method 4: Bulk density of aggregate. 2000, Standards-Australia.
37. ASTM C29 / C29M - 17a Standard Test Method for Bulk Density ("Unit Weight") and Voids in Aggregate. 2017, ASTM International: West Conshohocken, PA.
38. AS 1478.1-2000 Chemical admixtures for concrete, mortar and grout Admixtures for concrete. 2000, Standards-Australia.
39. ASTM C1437-15, Standard Test Method for Flow of Hydraulic Cement Mortar. 2015, ASTM International: West Conshohocken, PA.
40. ASTM C138 Standard Test Method for Density (Unit Weight), Yield, and Air Content (Gravimetric) of Concrete. 2017, ASTM International: West Conshohocken, PA.

41. ASTM C109 / C109M - 21 Standard Test Method for Compressive Strength of Hydraulic Cement Mortars (Using 2-in. or [50 mm] Cube Specimens). 2021, ASTM International: West Conshohocken.
42. AS 1012.13 Methods of testing concrete Determination of the drying shrinkage of concrete for samples prepared in the field or in the laboratory. 2015, Standards Australia.
43. Gartner E, Young J, Damidot D, et al., *Hydration of Portland cement*, in *Structure and Performance of Cements*. 2002, CRC Press. p. 57-108.
44. Farnam Y, Dick S, Wiese A, et al., The influence of calcium chloride deicing salt on phase changes and damage development in cementitious materials. *Cement and Concrete Composites*, 2015. **64**: p. 1-15.
45. Li P, Li W, Yu T, et al., Investigation on early-age hydration, mechanical properties and microstructure of seawater sea sand cement mortar. *Construction and Building Materials*, 2020. **249**: p. 118776.
46. Lothenbach B, Scrivener K and Hooton R, Supplementary cementitious materials. *Cement and Concrete Research*, 2011. **41**(12): p. 1244-1256.
47. Hjorth J, Skibsted J and Jakobsen HJ, 29Si MAS NMR studies of portland cement components and effects of microsilica on the hydration reaction. *Cement and Concrete Research*, 1988. **18**(5): p. 789-798.
48. Zain MFM, Safiuddin M and Yusof KM, A study on the properties of freshly mixed high performance concrete. *Cement and Concrete Research*, 1999. **29**(9): p. 1427-1432.
49. Turk K, Viscosity and hardened properties of self-compacting mortars with binary and ternary cementitious blends of fly ash and silica fume. *Construction and Building Materials*, 2012. **37**: p. 326-334.
50. Eide MB and Hisdal J-M, Ultra High Performance Fibre Reinforced Concrete (UHPFRC)–State of the art; 2012. (Coin Project Report–44).
51. Zhang J and Zhao Y, The mechanical properties and microstructure of ultra-high-performance concrete containing various supplementary cementitious materials. *Journal of Sustainable Cement-Based Materials*, 2017. **6**(4): p. 254-266.
52. Van Tuan N, Ye G, van Breugel K, et al., The study of using rice husk ash to produce ultra high performance concrete. *Construction and Building Materials*, 2011. **25**(4): p. 2030-2035.

53. Chen Y, Matalkah F, Soroushian P, et al., Optimization of ultra-high performance concrete, quantification of characteristic features. *Cogent Engineering*, 2019. **6**(1): p. 1558696.
54. Sakir S, Raman SN, Safiuddin M, et al., Utilization of By-Products and Wastes as Supplementary Cementitious Materials in Structural Mortar for Sustainable Construction. 2020. **12**(9): p. 3888.
55. Du H, Du S and Liu X, Durability performances of concrete with nano-silica. *Construction and Building Materials*, 2014. **73**: p. 705-712.
56. Zhang X and Zhang H, Experimental Research on Ultra-High Performance Concrete (UHPC). *IOP Conference Series: Materials Science and Engineering*, 2019. **562**(1): p. 012045.
57. Kuhail Z and Shihada S, Effect of Gaza seawater on concrete strength for different exposures. *IUG Journal for Natural Engineering Studies*, 2003. **11**(2).
58. Binici H, Aksogan O, Görür EB, et al., Performance of ground blast furnace slag and ground basaltic pumice concrete against seawater attack. *Construction and Building Materials*, 2008. **22**(7): p. 1515-1526.
59. Wu L, Farzadnia N, Shi C, et al., Autogenous shrinkage of high performance concrete: A review. *Construction and Building Materials*, 2017. **149**: p. 62-75.
60. Park SS, Kwon S-J and Song H-W, Analysis technique for restrained shrinkage of concrete containing chlorides. *Materials and Structures*, 2011. **44**(2): p. 475-486.
61. Dhondy T, Xiang Y, Yu T, et al., Effects of mixing water salinity on the properties of concrete. 2021. **24**(6): p. 1150-1160.
62. Yang E-I, Kim M-Y, Park H-G, et al., Effect of partial replacement of sand with dry oyster shell on the long-term performance of concrete. *Construction and Building Materials*, 2010. **24**(5): p. 758-765.
63. Li H, Farzadnia N and Shi C, The role of seawater in interaction of slag and silica fume with cement in low water-to-binder ratio pastes at the early age of hydration. *Construction and Building Materials*, 2018. **185**: p. 508-518.
64. Liu J, Shi C and Wu Z, Hardening, microstructure, and shrinkage development of UHPC: A review. *Journal of Asian Concrete Federation*, 2019. **5**(2): p. 1-19.
65. Lee KM, Lee HK, Lee SH, et al., Autogenous shrinkage of concrete containing granulated blast-furnace slag. *Cement and Concrete Research*, 2006. **36**(7): p. 1279-1285.

66. Hale WM, Freyne SF, Bush TD, et al., Properties of concrete mixtures containing slag cement and fly ash for use in transportation structures. *Construction and Building Materials*, 2008. **22**(9): p. 1990-2000.
67. AS 1379 Specification and supply of concrete. 2007, Standards Australia.

(a) (b)

Figure 1. Preparation and modification of sea sand (a) Impurities in sea sand, (b) sea sand after processing.

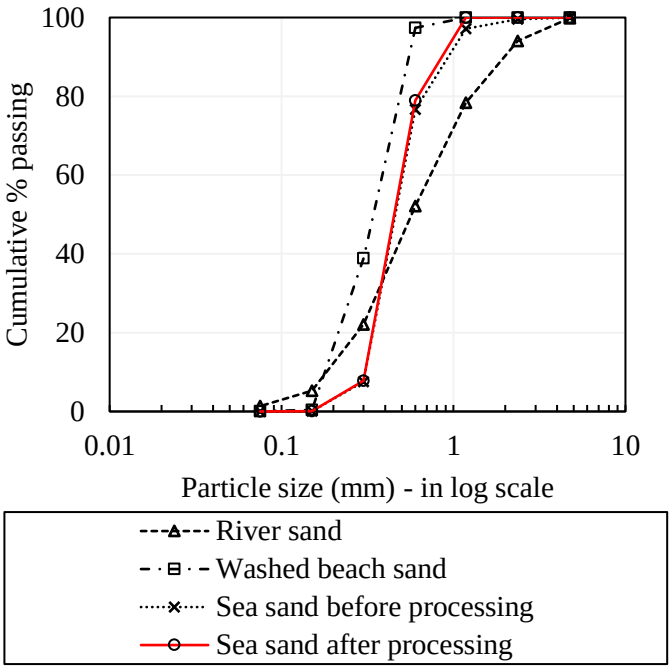

Figure 2. Particle size distribution curves of different sand aggregates (cumulative passing).

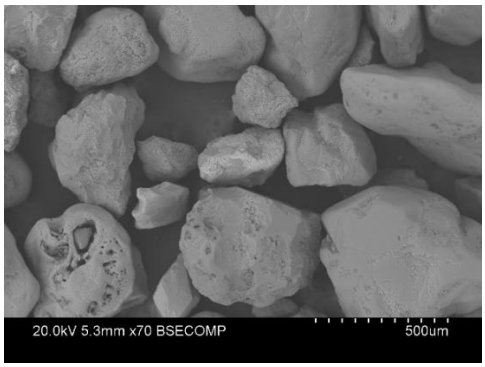

(a)

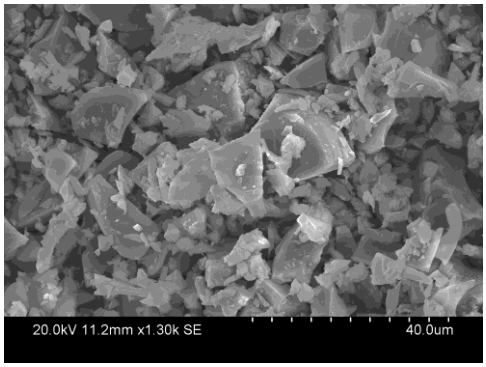

(d)

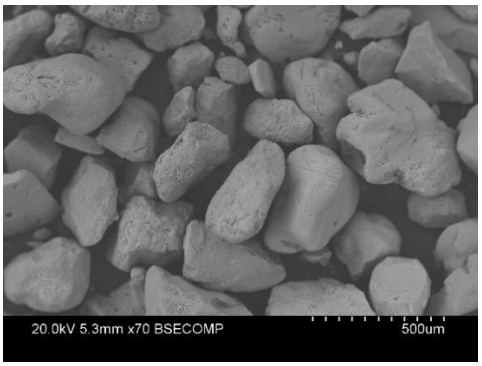

(b)

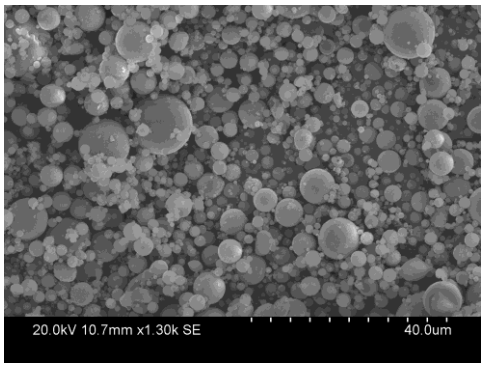

(e)

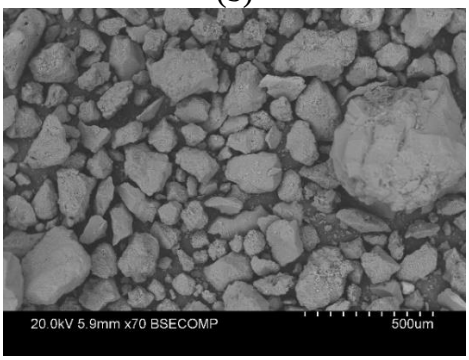

(c)

Figure 3. SEM images of different sand particles and SCMs (a) Sea sand, (b) washed beach sand, (c) river sand, (d) ground slag, (e) silica fume.

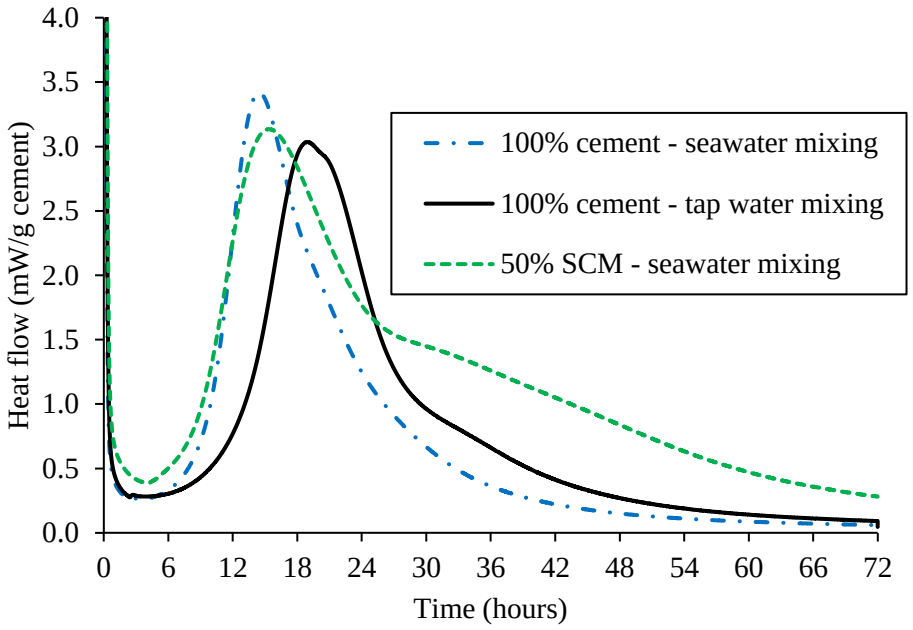

(a)

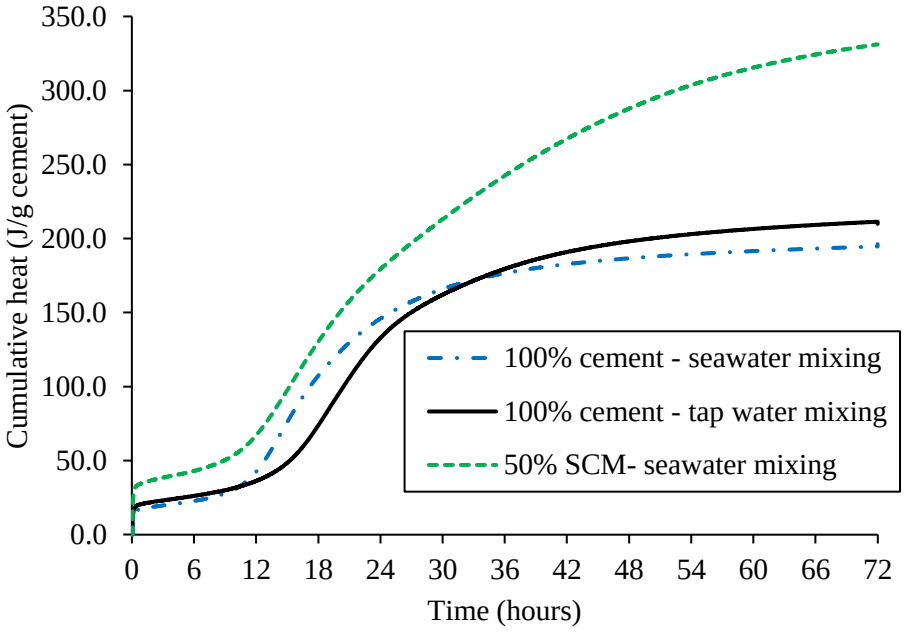

(b)

Figure 4. (a) Heat flow and (b) cumulative heat captured in an isothermal condition in the first 72 hours of hydration.

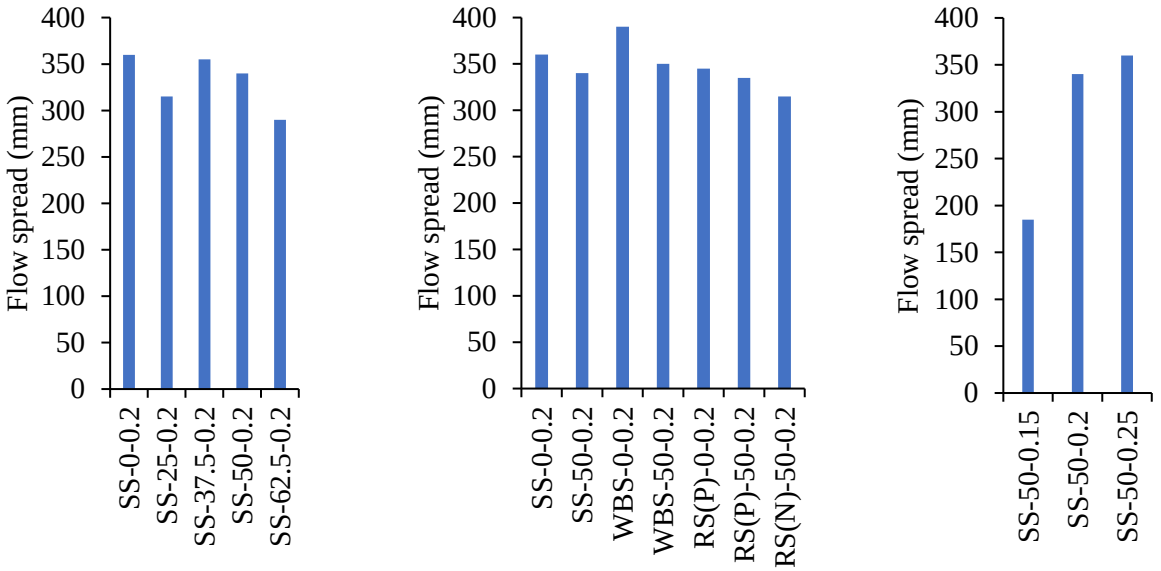

Figure 5. Comparison of workability of fresh UHP-SWSSC (by flow table test) based on (a) percentage of OPC replacement, (b) water to binder ratio, (c) different sand types.

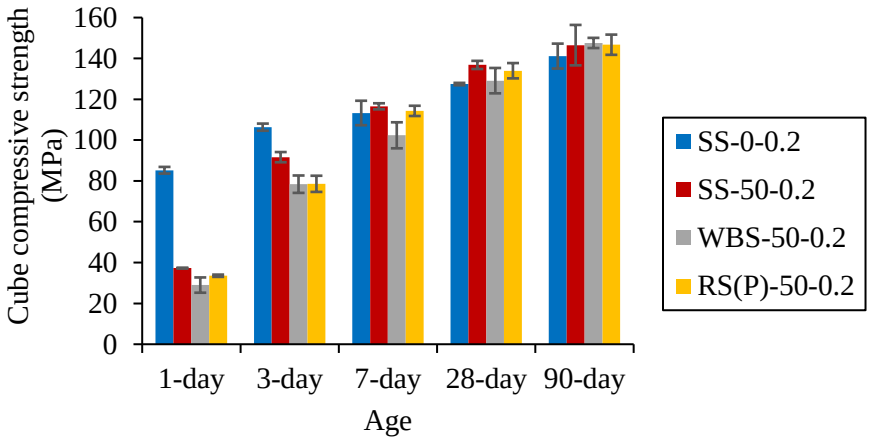

Figure 6. Effect of seawater and sea sand as mixing water and aggregate (tap water curing).

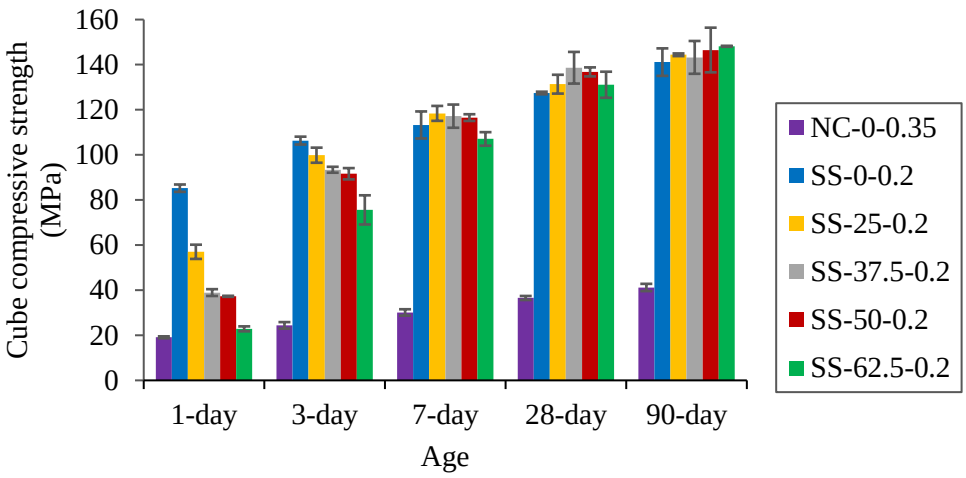

Figure 7. Effect of OPC replacement on cube compressive strength of UHP-SWSSC (tap water curing).

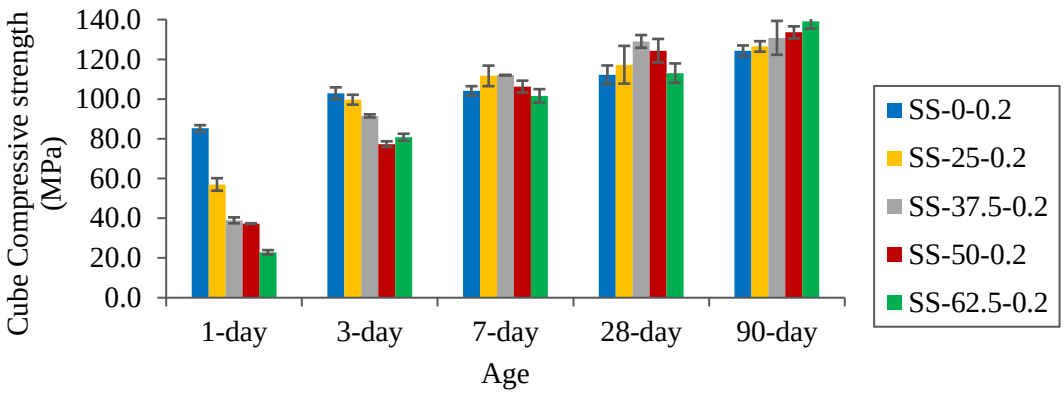

Figure 8. Effect of OPC replacement on cube compressive strength of UHP-SWSSC (seawater curing).

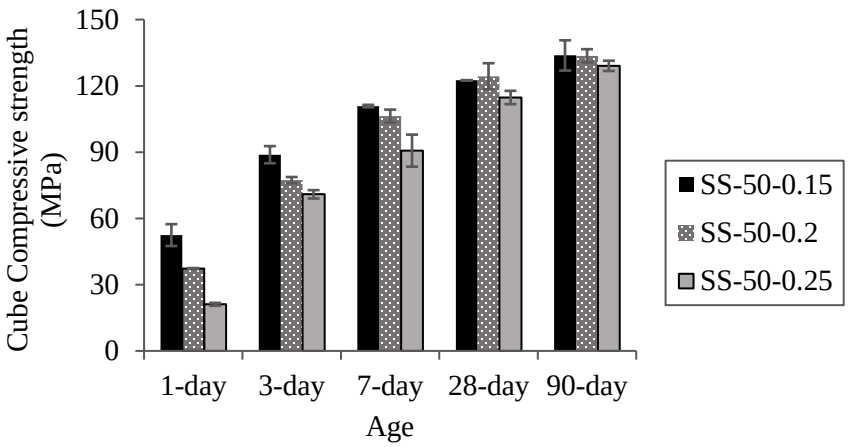

Figure 9. Effect of water to binder ratio on cube compressive strength (seawater curing).

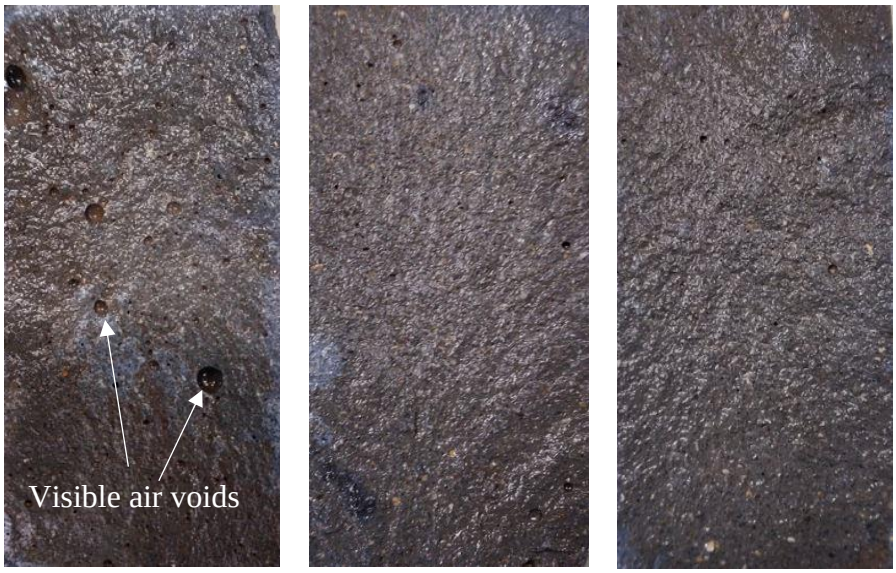

(a) (b) (c)

Figure 10. Cross-sections of UHP-SWSSC with different water to binder ratio (a) SS-50-0.15, (b) SS-50-0.2, (c) SS-50-0.25.

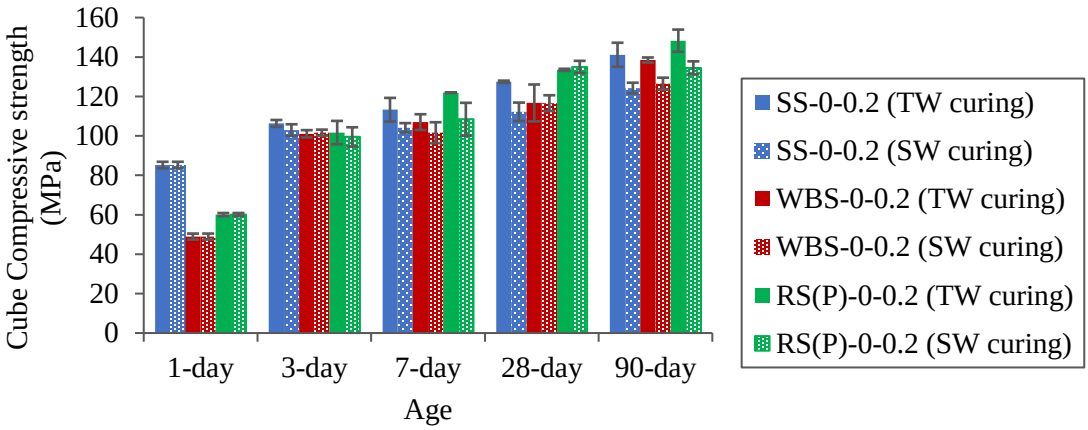

Figure 11. Effect of seawater curing on UHPC (100% OPC) with different aggregate types.

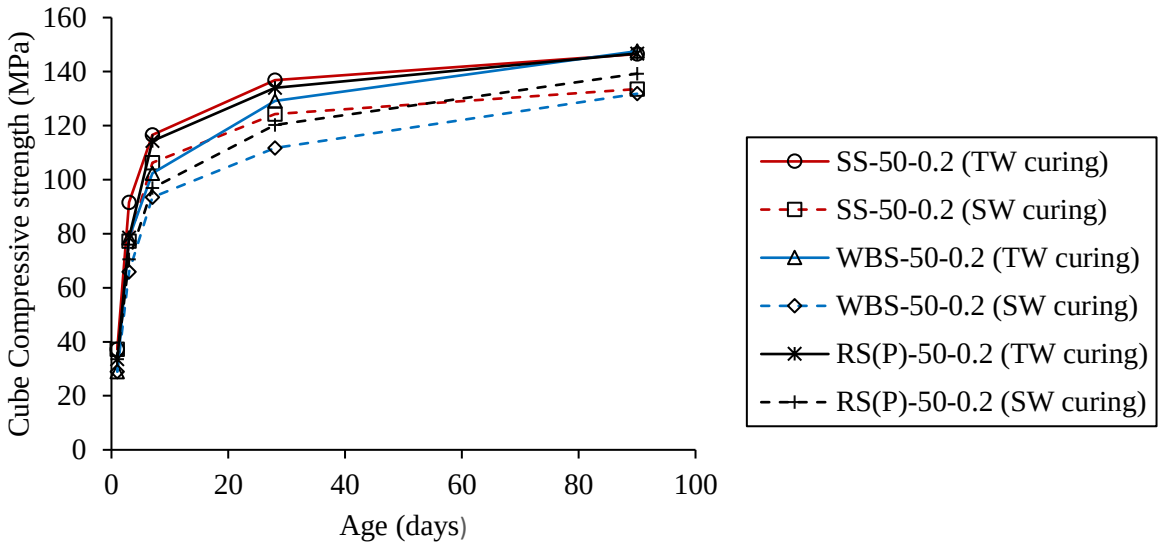

Figure 12. Effect of seawater curing on UHPC (50% OPC replacement) with different aggregate types.

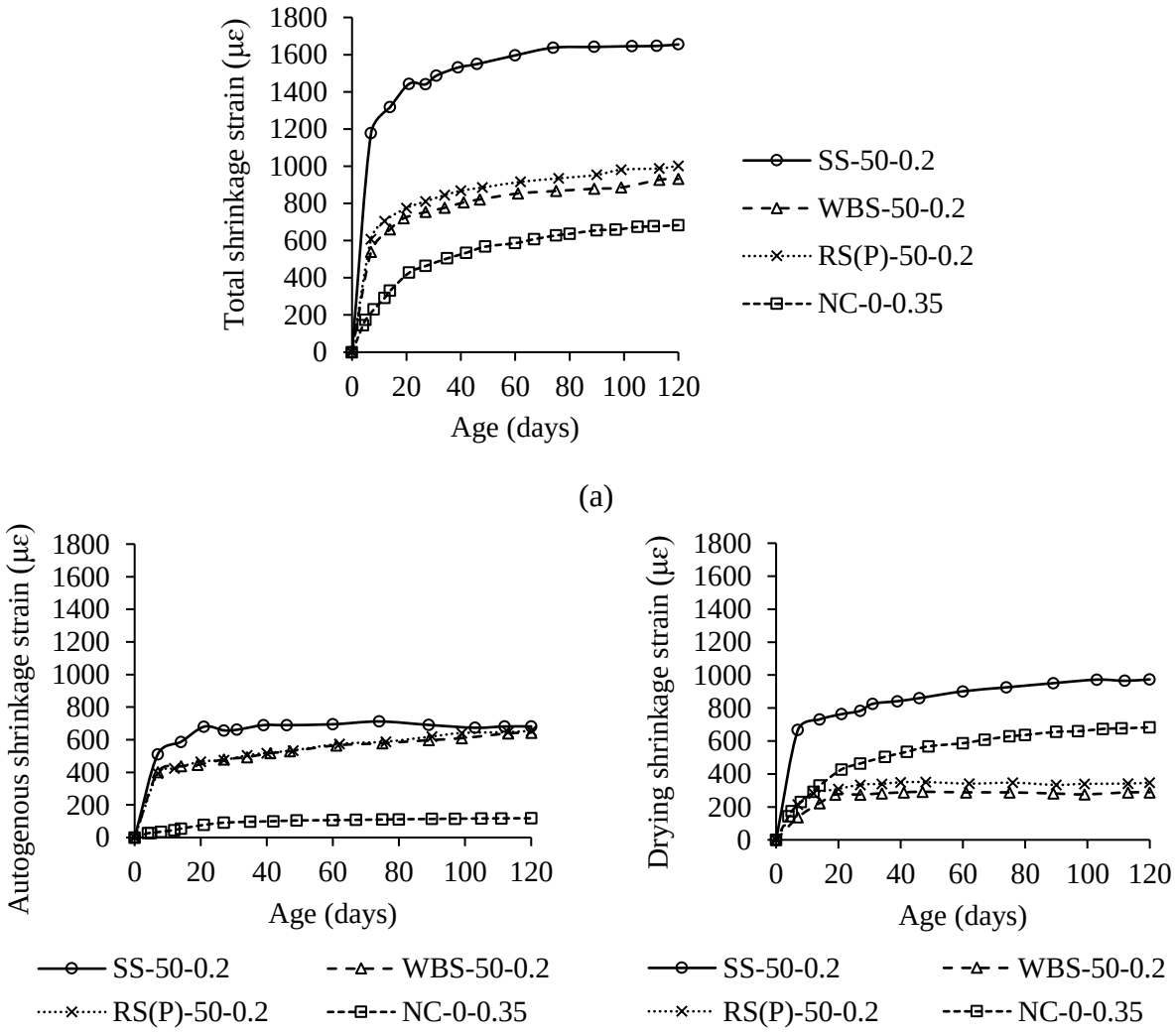

Figure 13. Effect of sand types on shrinkage of UHPC (a) Total shrinkage, (b) Autogenous shrinkage, (c) Drying shrinkage.

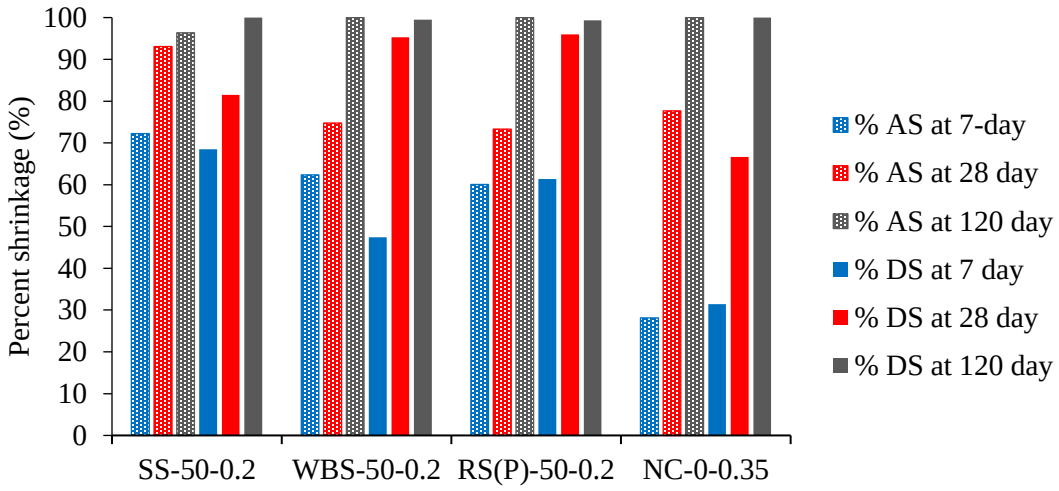

AS – autogenous shrinkage, DS – drying shrinkage.

Figure 14. Percentage of autogenous and drying shrinkage development among mixes with different types of sand.

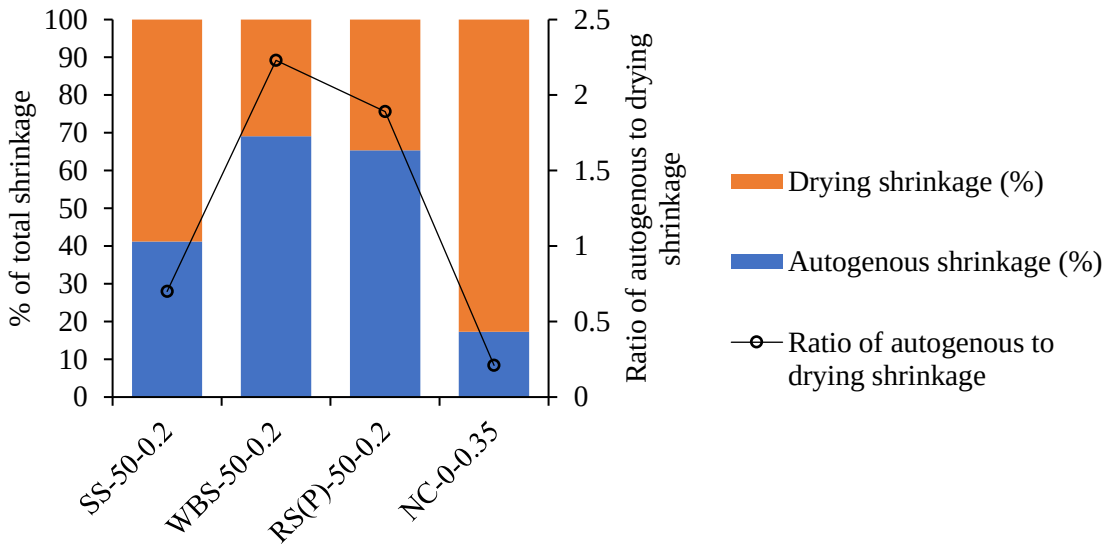

Figure 15. Proportions of autogenous and drying shrinkage at 120 days (different types of sand).

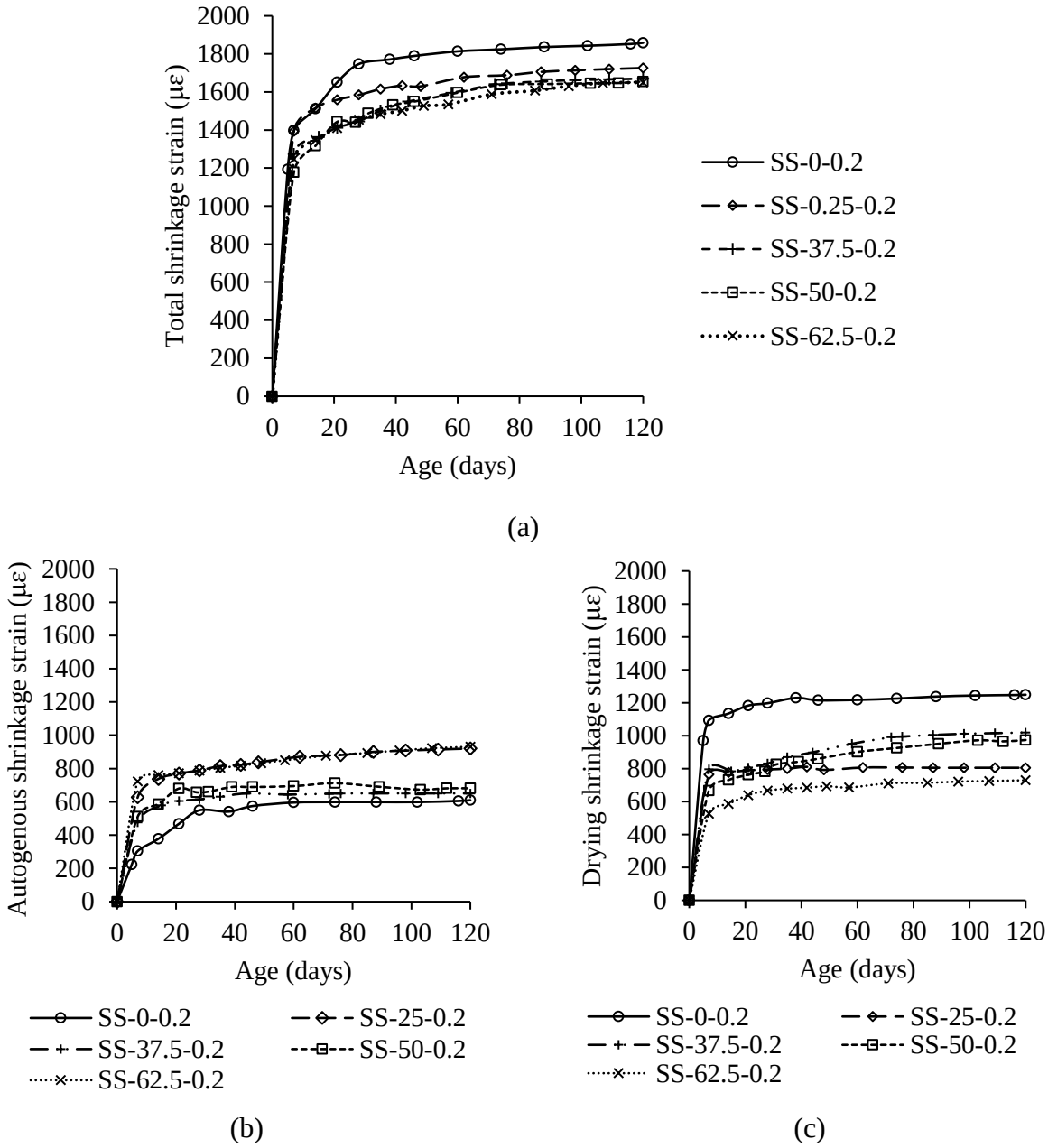

Figure 16. Influence of OPC replacement on shrinkage of UHPC (a) Total shrinkage, (b) Autogenous shrinkage, (c) Drying shrinkage.

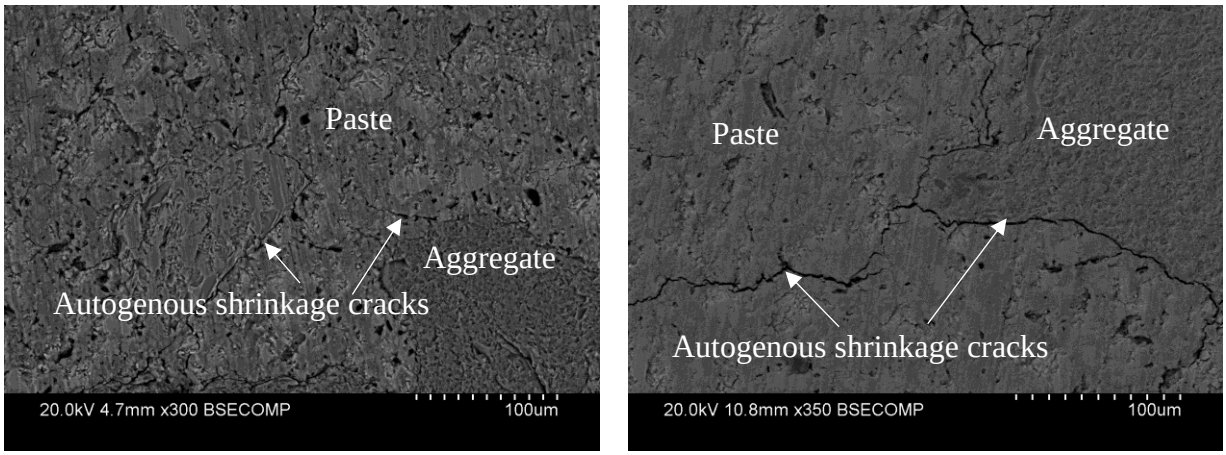

(a) (b)

Figure 17. Autogenous shrinkage cracks in the microstructure of UHPC (a) 100% OPC, (b) 25% OPC replaced by slag.

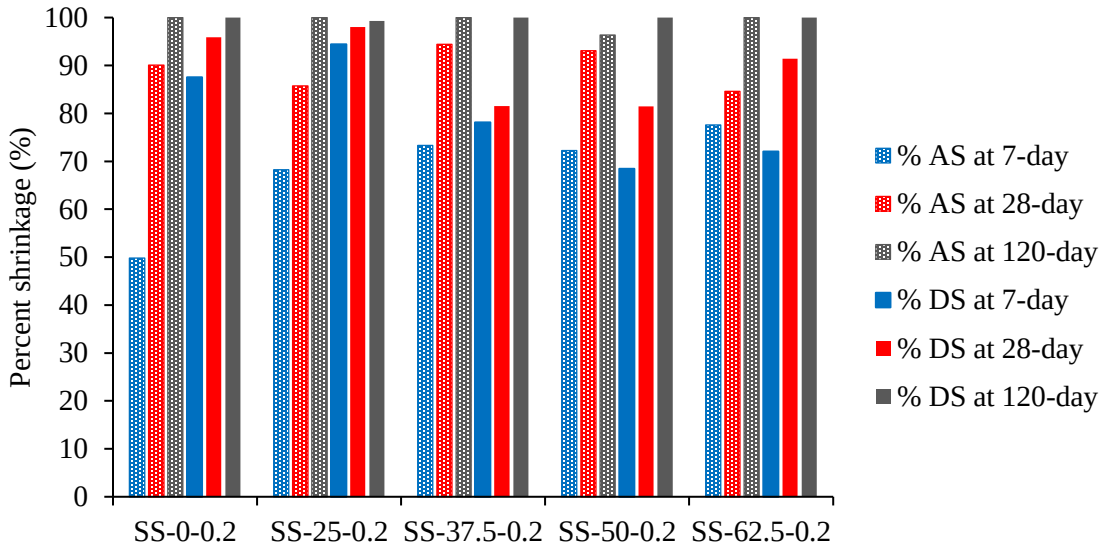

AS – autogenous shrinkage, DS – drying shrinkage.

Figure 18. Percentage of autogenous and drying shrinkage development among mixes with different OPC replacement.

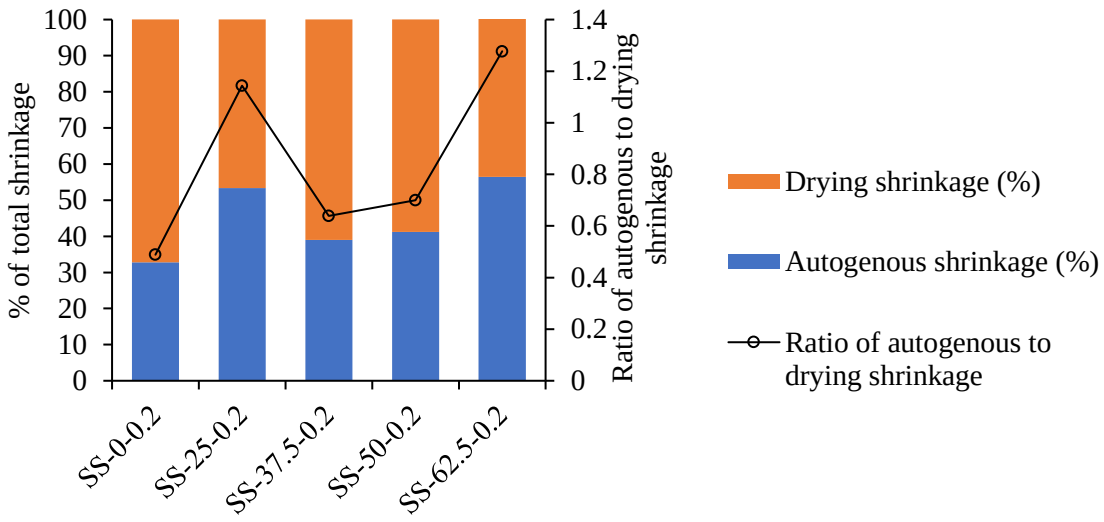

Figure 19. Proportions of autogenous and drying shrinkage at 120 days (percentage of OPC replacement).

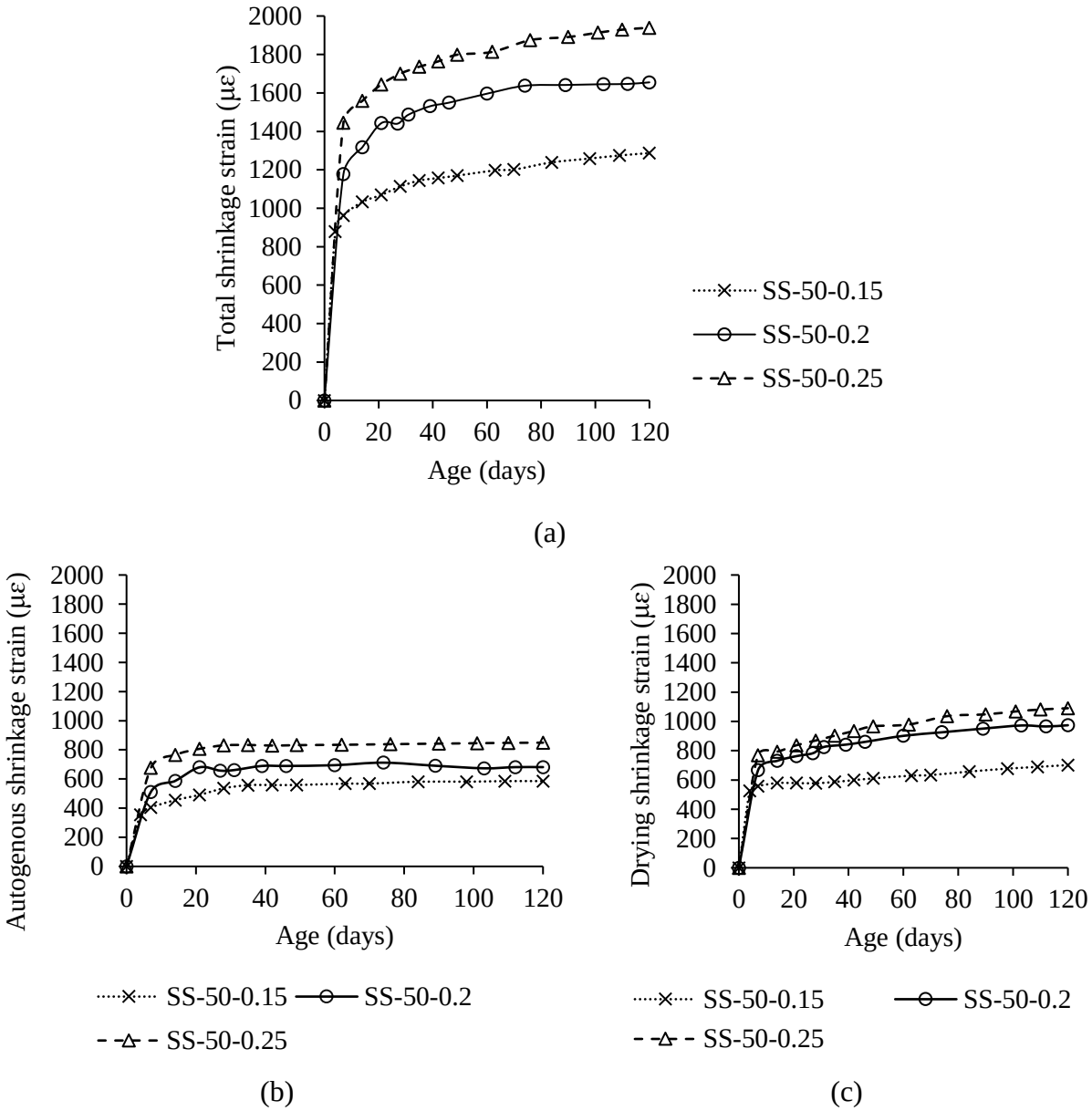

Figure 20. Influence of water-to-binder ratio on shrinkage of UHPC (a) Total shrinkage, (b) Autogenous shrinkage, (c) Drying shrinkage.

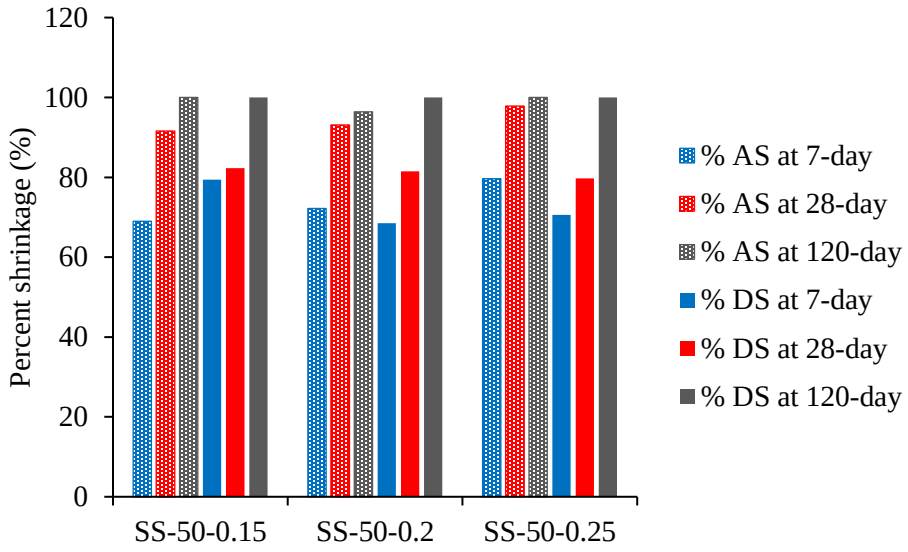

AS – autogenous shrinkage, DS – drying shrinkage.

Figure 21. Percentage of autogenous and drying shrinkage development among mixes with different water to binder ratio.

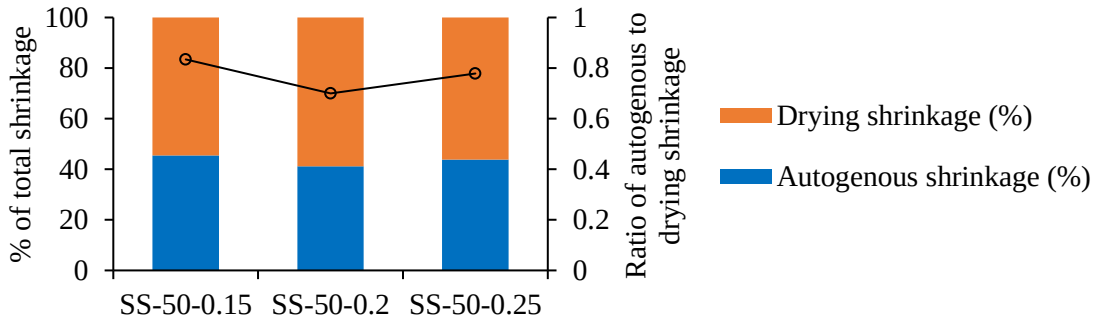

Figure 22. Proportions of autogenous and drying shrinkage at 120 days (water to binder ratio).

Figure captions

Table 1. Chemical compositions of cementitious materials.

Chemical properties (wt. %)	Portland cement	GGBFS	Silica fume
SiO_2	19.37	32.13	92.18
Al_2O_3	4.88	13.66	0.09
Fe_2O_3	3.4	0.36	0.01
CaO	63.45	42.56	0.1
MgO	0.88	5.51	0.28
Na_2O	0.48	0.31	0.22
K_2O	0.37	0.31	0.26
TiO_2	0.31	0.54	<0.01
SO_3	2.36	3.24	0.01
P_2O_5	0.06	0.01	0.1
Mn_3O_4	0.05	0.15	<0.01
Loss on ignition (LOI)	4.25	0.95	6.25

Table 2. Chemical compositions of natural seawater.

Ion (in mg/L)	Natural seawater from Malabar, NSW	World average of seawater Teng et al. [29]
F^-	10.6	1.3
Cl^-	19131	19352
Br^-	71.7	67.3
SO_4^{2-}	2658	2712
PO_4^{3-}	nil	nil
NO_2^-	nil	nil
NO_3^-	nil	nil
Li^+	0.296	nil
Na^+	10691	10784
Mg^{2+}	891.6	1283.7
Al^{3+}	0.112	nil
Si^{4+}	0.140	nil
K^+	427.4	399.1
Ca^{2+}	419.5	412.1
Fe^{2+}	0.002	nil

Table 3. Chemical compositions of different types of sand.

Chemical properties (wt. %)	Sea sand	Washed beach sand	River sand
SiO_2	88.80	86.00	95.90
Al_2O_3	0.70	1.00	1.08
Fe_2O_3	0.44	0.28	0.23
CaO	4.58	5.32	0.03
MgO	0.17	0.16	<0.01
Na_2O	0.20	0.20	0.01
K_2O	0.12	0.35	0.18
TiO_2	0.06	0.03	0.08
SO_3	0.04	0.02	<0.01
P_2O_5	0.02	0.02	<0.01
Mn_3O_4	<0.01	<0.01	<0.01
SrO	0.03	0.02	0.04
Loss on ignition (LOI)	4.26	5.05	0.85

Table 4. Physical properties of different types of sand.

Physical properties	Sea sand	Washed beach sand	River sand (natural)	River sand (processed)
Oven dry density (t/m^3)	2.41	2.44	2.51	2.41
SSD density (t/m^3)	2.50	2.51	2.55	2.46
Apparent density (t/m^3)	2.63	2.63	2.62	2.55
Uncompacted bulk density (t/m^3)	1.47	1.42	1.50	1.47
Compacted bulk density (t/m^3)	1.68	1.62	1.76	1.67
Water absorption (%)	3.46	2.95	1.68	2.35
Void (%)	38.94	41.73	40.42	39.04

Table 5. Mixture proportions of materials for UHPC and normal strength concrete.

Mix ID	Replacement of OPC (%)	Aggregate	Mixing water	Water to binder ratio	OPC kg/m^3	Ground Slag kg/m^3	Silica fume kg/m^3	Sand kg/m^3	Coarse aggregate kg/m^3	Water kg/m^3	HRWR kg/m^3
SS-0-0.2	0	Sea sand	Seawater	0.2	1200	0	0	1000	N/A	240	24
SS-25-0.2	25	Sea sand	Seawater	0.2	900	300	0	1000	N/A	240	24
SS-37.5-0.2	37.5	Sea sand	Seawater	0.2	750	300	150	1000	N/A	240	24
SS-50-0.2	50	Sea sand	Seawater	0.2	600	450	150	1000	N/A	240	24
SS-62.5-0.2	62.5	Sea sand	Seawater	0.2	450	600	150	1000	N/A	240	24
SS-50-0.15	50	Sea sand	Seawater	0.15	615	461.3	153.7	1025	N/A	184.5	24.6
SS-50-0.25	50	Sea sand	Seawater	0.25	585.7	439.3	146.4	976.2	N/A	292.9	23.43
WBS-0-0.2	0	Washed beach sand	Tap water	0.2	1200	0	0	1000	N/A	240	24
WBS-50-0.2	50	Washed beach sand	Tap water	0.2	600	450	150	1000	N/A	240	24
RS(P)-0-0.2	0	River sand (processed)	Tap water	0.2	1200	0	0	1000	N/A	240	24
RS(N)-50-0.2	50	River sand (natural)	Tap water	0.2	600	450	150	1000	N/A	240	24
RS(P)-50-0.2	50	River sand (processed)	Tap water	0.2	600	450	150	1000	N/A	240	24
NC-0-0.35	0	Washed beach sand	Tap water	0.35	380	0	0	1102	840	133	1.9

SS – Sea sand, WBS – Washed beach sand, RS(P) – Processed river sand, RS(N) – Natural river sand, NC – Normal strength concrete.

Table 6. Fresh and SSD unit weight of UHPC and normal strength concrete.

Mix ID	Fresh density kg/m^3	SSD density kg/m^3
SS-0-0.2	2400.8	2421.0
SS-25-0.2	2373.3	2392.0
SS-37.5-0.2	2316.8	2335.4
SS-50-0.2	2305.0	2323.0
SS-62.5-0.2	2304.8	2315.8
SS-50-0.15	2308.6	2315.4
SS-50-0.25	2247.5	2264.8
WBS-0-0.2	2392.3	2424.4
WBS-50-0.2	2285.1	2291.2
RS(P)-0-0.2	2379.4	2394.2
RS(N)-50-0.2	2322.2	2338.1
RS(P)-50-0.2	2264.3	2299.1
NC-0-0.35	2252.2	2270.8

SS – Sea sand, WBS – Washed beach sand, RS(P) – Processed river sand, RS(N) – Natural river sand, NC – Normal strength concrete.

Table 7. Compressive strength of UHPC and normal strength concrete (cube specimens).

Mix ID	Curing water	1 day (MPa)		3 days (MPa)		7 days (MPa)		28 days (MPa)		90 days (MPa)	
		Mean	SD	Mean	SD	Mean	SD	Mean	SD	Mean	SD
SS-0-0.2	TW curing	85.23	1.63	106.33	1.74	113.27	6.00	127.43	0.58	141.13	6.10
	SW curing			102.93	2.96	104.10	2.36	112.20	4.69	124.27	2.70
SS-25-0.2	TW curing	57.01	3.16	99.86	3.35	118.40	3.31	131.35	4.17	144.39	0.59
	SW curing			99.67	2.48	111.66	5.17	117.27	9.48	126.47	2.66
SS-37.5-0.2	TW curing	38.94	1.51	93.40	1.31	117.17	5.15	138.63	7.02	143.23	7.27
	SW curing			91.50	0.78	112.03	0.15	129.00	3.20	130.80	8.52
SS-50-0.2	TW curing	37.28	0.22	91.63	2.50	116.53	1.48	136.80	2.00	146.50	9.90
	SW curing			77.30	1.41	106.30	2.94	124.33	5.92	133.55	3.04
SS-62.5-0.2	TW curing	22.85	1.10	75.60	6.47	107.07	3.00	131.10	5.79	148.15	0.21
	SW curing			80.77	1.76	101.60	3.39	113.07	4.87	139.10	3.67
SS-50-0.15	TW curing	52.43	4.95	91.67	3.88	112.50	0.56	128.05	0.07	140.25	6.86
	SW curing			88.83	9.67	110.83	6.43	122.50	3.80	133.77	1.05
SS-50-0.25	TW curing	21.09	0.67	73.03	1.90	94.43	7.25	124.20	3.01	128.97	2.32
	SW curing			70.89	2.80	90.67	8.14	114.73	7.58	129.05	0.35
WBS-0-0.2	TW curing	48.93	1.51	101.07	1.85	106.97	4.01	116.70	9.35	138.47	1.29
	SW curing			101.59	1.59	101.60	5.31	116.60	4.00	126.47	3.04
WBS-50-0.2	TW curing	28.98	3.74	78.40	4.26	102.33	6.38	129.10	6.21	147.57	2.50
	SW curing			65.83	1.71	93.43	4.40	111.70	9.81	131.80	4.00
RS(P)-0-0.2	TW curing	60.07	0.81	101.68	5.91	121.90	0.14	133.50	0.53	148.30	5.62
	SW curing			99.47	4.90	108.43	8.33	134.97	3.08	134.50	3.31
RS(N)-50-0.2	TW curing	28.78	0.80	76.80	0.80	103.73	8.17	131.53	5.98	142.27	6.82
	SW curing			74.53	1.15	95.97	2.25	113.00	10.65	130.07	1.50
RS(P)-50-0.2	TW curing	33.55	0.56	78.58	3.96	114.30	2.51	133.97	3.75	146.70	4.95
	SW curing			70.45	3.59	96.90	1.13	120.20	5.71	139.23	2.50
NC-0-0.35	TW curing	19.10	0.43	24.40	1.44	30.13	1.41	36.54	0.89	41.20	1.61

SS – Sea sand, WBS – Washed beach sand, RS (P) – Processed river sand, RS (N) – Natural river sand, NC – Normal strength concrete, TW – Tap water, SW – Seawater, SD – Standard deviation.

Table 8. Percentage variation of physical, mechanical and stability properties of different mixes compared to reference UHP-SWSSC.

Mix ID	Variation in Unit weight		Variation in workability	Variation in compressive strength (seawater curing)			Variation in maximum shrinkage		
	Fresh unit weight	28-day unit weight		1-day	28-day	90-day	AS	DS	TS
SS-0-0.2	0%	0%	0%	0%	0%	0%	0%	0%	0%
SS-25-0.2	-1.14%	-1.20%	-12.50%	-33.11%	+4.52%	+1.77%	+50.90%	-35.07%	-7.15%
SS-37.5-0.2	-3.50%	-3.53%	-1.39%	-54.32%	+14.97%	+5.26%	+6.72%	-18.37%	-10.14%
SS-50-0.2	-3.99%	-4.04%	-5.56%	-56.26%	+10.81%	+7.47%	+15.92%	-22.01%	-10.95%
SS-62.5-0.2	-4.00%	-4.34%	-19.44%	-73.19%	+0.77%	+11.94%	+52.64%	-41.60%	-10.67%
SS-50-0.15	-3.84%	-4.36%	-48.61%	-38.48%	+9.18%	+7.64%	-4.05%	-43.80%	-30.76%
SS-50-0.25	-6.38%	-6.45%	0%	-75.25%	+2.26%	+3.85%	+39.18%	-12.70%	+4.33%
WBS-50-0.2	-4.82%	-5.36%	-2.78%	-66.00%	-0.45%	+6.06%	+5.48%	-76.82%	-49.88%
RS(P)-50-0.2	-5.68%	-5.03%	-6.94%	-60.63%	+7.13%	+12.04%	+7.38%	-71.99%	-46.07%
NC-0-0.35	-6.19%	-6.20%	N/A	-77.59%	-67.43%	-66.85%	-80.60%	-54.78%	-63.26%

AS – autogenous shrinkage, DS – drying shrinkage, TS – total shrinkage.

NC-0-0.35 was cured in tap water.

A positive (+) value indicates an increase, and a negative (-) value indicates a decrease.